

MOX–Report No. 59/2014

**Accurate solution of Bayesian inverse uncertainty
quantification problems using model and error
reduction methods**

MANZONI, A.; PAGANI, S.; LASSILA, T.

MOX, Dipartimento di Matematica “F. Brioschi”
Politecnico di Milano, Via Bonardi 9 - 20133 Milano (Italy)

mox@mate.polimi.it

<http://mox.polimi.it>

Accurate solution of Bayesian inverse uncertainty quantification problems using model and error reduction methods*

A. Manzoni[†] S. Pagani[‡] T. Lassila[§]

November 21, 2014

Abstract

Computational inverse problems related to partial differential equations (PDEs) often contain nuisance parameters that cannot be effectively identified but still need to be considered as part of the problem. The objective of this work is to show how to take advantage of projection-based reduced order models (ROMs) to speed up Bayesian inversion on the identifiable parameters of the system, while marginalizing away the (potentially large number of) nuisance parameters. The key ingredients are twofold. On the one hand, we rely on a reduced basis (RB) method, equipped with computable a posteriori error bounds, to speed up the solution of the forward problem. On the other hand, we develop suitable reduction error models (REM) to quantify the error between the full-order and the reduced-order model affecting the likelihood function, in order to gauge the effect of the ROM on the posterior distribution of the identifiable parameters. Numerical results dealing with inverse problems governed by elliptic PDEs in the case of both scalar parameters and parametric fields highlight the combined role played by ROM accuracy and REM effectivity.

1 Introduction

The efficient solution of inverse problems governed by PDEs is a relevant challenge from both a theoretical and a computational standpoint. In these problems, unknown or uncertain parameters related to a PDE model have to be estimated from indirect observations of suitable quantities of interest. Being able to design efficient numerical procedures to solve inverse problems plays a key role in several applications, ranging from life sciences (e.g., in electrical impedance tomography [24, 30], characterization of myocardial ischemias and identification of blood flow parameters [35, 19]), to material sciences (e.g. scattering problems [7] or subsurface damage detection [3]) and environmental sciences (e.g., identification of permeability in groundwater flows [27], or basal sliding in ice dynamics [31]).

In a parametrized context, a forward problem consists in evaluating some outputs of interest (depending on the PDE solution) for specified parameter inputs. Whenever some parameters are uncertain, they can be identified by considering either a deterministic or a statistical framework. In the former case, we solve an optimization problem by minimizing (e.g. in the least-square sense) the *discrepancy* between the output quantities predicted by the PDE model and the observations. In the latter case, we assess the relative likelihood of the parameters which are consistent with the observed

*We are grateful to Prof. Anna Maria Paganoni (Politecnico di Milano) for her valuable insights and careful remarks, and to Prof. Alfio Quarteroni (EPFL and Politecnico di Milano) for his useful suggestions. This work was supported by “National Group of Computing Science” (GNCS-INDAM).

[†]CMCS-MATHICSE-SB, Ecole Polytechnique Fédérale de Lausanne, Station 8, CH-1015 Lausanne, Switzerland, andrea.manzoni@epfl.ch (corresponding author)

[‡]MOX, Dipartimento di Matematica, Politecnico di Milano, P.za Leonardo da Vinci 32, I-20133 Milano, Italy, stefano.pagani@polimi.it

[§]CISTIB, Department of Mechanical Engineering, University of Sheffield, Mappin Street, Sheffield S1 3JD, United Kingdom, t.lassila@sheffield.ac.uk

output, that is, we need to quantify uncertainties associated with the identifiable parameters due to measurement errors and to nuisance parameters. Such a problem can be referred to as *inverse uncertainty quantification (UQ)* problem. By relying on a *Bayesian approach*, we model the unknown parameters as random variables and characterize their *posterior* probability density function, which includes information both on *prior* knowledge on the parameters distribution and on the model used to compute the PDE-based outputs [36]. In this way, inference of unknown parameters from noisy data accounts for the information coming from (possibly complex and nonlinear) physical models [37, 17]. Nevertheless, we need to face some key numerical challenges, related to parametric dimensionality, many forward queries and slow Markov chain Monte Carlo (MCMC) convergence. While the first issue can be addressed by considering a parametric reduction (e.g. through a modal decomposition exploiting a Karhunen-Loève expansion [24] or suitable greedy algorithms [23]), several techniques have emerged in the last decade to speed up either *(ii)* the solution of the forward problem, or *(iii)* MCMC sampling algorithms, see e.g. [26, 21] and references therein. Quasi-Monte Carlo methods or sparse grid techniques [11] also provide feasible options when dealing with this class of problems.

In this work we focus on computational reduction to speed up the solution of Bayesian inverse problems, for which either low-fidelity or surrogate models can be exploited [4]. A low-fidelity model can be built according to simplified physics, coarser discretizations, multiscale formulations or reduced-order approximations. Such a model can also be equipped with correction functions using global polynomials in term of the stochastic parameters. For instance, non-intrusive polynomial chaos using orthogonal polynomials [13] and stochastic collocation using interpolation polynomials [2, 38] have been developed in conjunction with physics-based low fidelity models, e.g. in [29]. Here we focus instead on low-dimensional, *projection-based reduced-order models (ROMs)* built by combining few high-fidelity solutions for properly selected parameter values. In this way, each forward query is inexpensive and the overall computational cost entailed by the Bayesian inversion can be greatly reduced. Among projection-based ROMs, certified reduced basis (RB) methods [4, 19] or proper orthogonal decomposition (POD) [12, 24, 27, 34] have been already successfully exploited in this field during the last decade. Very recently, a possible way to compute snapshots adaptively from the posterior distribution, yielding a data-driven ROM, has been shown in [9]. Also proper generalized decomposition has been combined with stochastic spectral methods in order to characterize dynamical systems in the presence of stochastic parametric uncertainties [8].

A relevant question, arising when surrogate models or ROMs are exploited to solve inverse problems, is related to the propagation of *reduction errors* along the inversion process. In other words, we need to quantify those uncertainties due to the ROM and associated with the identifiable parameters, to which we refer to as *ROM uncertainty*. This latter can be seen as a form of *epistemic uncertainty*, and its quantification is essential in order to obtain precise and robust solutions to the Bayesian inverse UQ problem¹. Concerning the role of ROM uncertainty, two approaches have been considered very recently: the so-called approximation error model [1, 24], and Gaussian process (GP)-based calibration (or GP machine learning) [34]. In both cases, a statistical representation of the ROM error through the calibration experiments is used to model the difference between the higher-fidelity and the lower-fidelity model. In the first case an additive Gaussian noise is introduced in the model to represent the reduction error; in the second case a Gaussian process is used, estimating the covariance function through the calibration experiments. However, error characterization through well-defined probability distributions may impose a large amount of (sometimes unjustified) statistical structure, thus leading to inaccurate results. For instance, in the approximation error model the uncertainty yielded by the ROM is described as an independent Gaussian error term, which might be a restrictive assumption (see Sect.7). On the other hand, GP machine learning techniques entail more severe computational costs; a possible reduction technique in this context has been recently presented in [10] and takes advantage of a posteriori error bounds, weighted with a Gaussian process to generate a more accurate correction. The reduction error model (REM-3) we introduce in Sect. 4.3 shares some similarities with this approach, but

¹ROM uncertainty is similar to the so-called *model form uncertainty*, arising when a limited understanding of the modeled process is available, see e.g. [16, 15] for further details about epistemic uncertainties.

enables variance estimations directly from a regression analysis and an easier treatment of sign effects/corrections, this last aspect being not covered in [10].

Our goal is to retain the positive features of most of these approaches by exploiting rigorous a posteriori error estimators, in order to quantify the reduction error within the Bayesian inversion process through suitable *reduction error models* (REMs). By extending some preliminary ideas presented in [19], we show how to take advantage of a certified RB method to gain a strong computational speedup. We propose three reduction error models (REMs) to manage ROM uncertainties. First, we exploit the approximation error model of Kaipio et al. [1], which however may perform quite poorly when dealing with problems involving nuisance parameters and/or error empirical distributions far from the Gaussian case. Then, we present two alternatives. In the first one, a radial basis interpolant allows to evaluate a surrogate reduction error over the parameter space, relying on few calibration experiments. In the second one, we fit a linear regression model to explain the variability of the reduction errors by means of the corresponding error bounds. In both cases, we show how reduction errors can be properly included within the Bayesian computational framework.

The structure of the paper is as follows. In Sect. 2 we provide a general formulation of the class of problems we are interested to, whereas in Sect. 3 we recall the main properties of RB methods. In Sect. 4, we introduce the three reduced error models considered, and we show how to incorporate them into the Bayesian estimator and in Sect. 5 we sum up the proposed computational procedure for the solution of a reduced inverse problem. In Sect. 6 we prove some results related to the effectivity of the corrections made by the REMs, on the reduced-order likelihood function and the corresponding posterior distribution. Finally, we show the properties and the performance of the correction strategies by presenting two numerical examples of inverse problems governed by elliptic PDEs in Sect. 7.

2 Bayesian inverse problems governed by PDEs

Let us introduce the abstract formulation of the forward problem modeling our system of interest, and recall the basic features of the Bayesian framework for the solution of inverse problems governed by PDEs.

2.1 Abstract formulation of forward problem

In this paper we consider systems modelled by linear parametrized PDEs and (a set of) linear outputs of interest. Let us denote by X a Hilbert space of functions defined over a domain $\Omega \subset \mathbb{R}^d$, $d = 1, 2, 3$. In the case of second-order, elliptic PDE operators typically $(H_0^1(\Omega))^\nu \subset X \subset (H^1(\Omega))^\nu$, where $\nu = 1$ (resp. $\nu = d$) in the case of scalar (resp. vectorial) problems. Here we restrict ourselves to the scalar case; the extension to the vectorial case is straightforward, concerning the formulation of an inverse problem. The forward problem depends on a finite-dimensional set of parameters $\boldsymbol{\mu} \in \mathcal{P} \subset \mathbb{R}^P$. Its abstract formulation reads as follows: given $\boldsymbol{\mu} \in \mathcal{P}$, find $u(\boldsymbol{\mu}) \in X$ such that

$$\begin{cases} a(u(\boldsymbol{\mu}), v; \boldsymbol{\mu}) = f(v; \boldsymbol{\mu}) & \forall v \in X & \text{(state equation)} \\ \mathbf{s}(\boldsymbol{\mu}) = \boldsymbol{\ell}(u(\boldsymbol{\mu})) & & \text{(observation equation).} \end{cases} \quad (1)$$

Here $a : X \times X \times \mathcal{P} \rightarrow \mathbb{R}$ and $f : X \times \mathcal{P} \rightarrow \mathbb{R}$ are a parametrized bilinear (resp. linear) form, $\mathbf{s} : \mathcal{P} \rightarrow \mathbb{R}^s$ and $\boldsymbol{\ell} = (\ell^1, \dots, \ell^s)$, being $\ell^j : X \rightarrow \mathbb{R}$ a linear form for any $j = 1, \dots, s$. This assumption is not as restrictive as one would think, since for example field-valued inverse problems can be treated by discretizing the underlying field with sufficient accuracy ($P \gg 1$) or by employing a truncated Karhunen-Loève expansion. In particular, we assume that the parameter vector is divided into two parts: $\boldsymbol{\mu} = (\boldsymbol{\gamma}, \boldsymbol{\zeta}) \in \mathbb{R}^{P_\gamma + P_\zeta}$; we denote by $\boldsymbol{\gamma}$ the *identifiable parameters*, and by $\boldsymbol{\zeta}$ the *nuisance parameters*. For the cases at hand, both identifiable and nuisance parameters will be related to physical properties of the system, thus entering the differential operator and possibly boundary conditions and source terms. See e.g. [19] for further details about the case of geometrical parameters.

We require that the forward problem is well-posed for any choice of the parameter vector $\boldsymbol{\mu} \in \mathcal{P}$. To this aim, we assume that $a(\cdot, \cdot; \boldsymbol{\mu})$ is continuous and uniformly coercive over X , for any $\boldsymbol{\mu} \in \mathcal{P}$, and that $f(\cdot; \boldsymbol{\mu})$ is continuous, that is, $f(\cdot; \boldsymbol{\mu}) \in X'$ for any $\boldsymbol{\mu} \in \mathcal{P}$, being X' the dual space of X . We also require that $\ell^j \in X'$ for any $j = 1, \dots, s$. The Lax-Milgram lemma ensures uniqueness of the solution (and its continuous dependence from data) for any $\boldsymbol{\mu} \in \mathcal{P}$. This framework can also be adapted to stable problems in the sense of an *inf-sup* condition, by using the Babuška-Nečas theorem; see e.g. [32] for further details.

A numerical approximation of the forward problem (1) can be obtained by introducing, e.g. a Galerkin-finite element (FE) method relying on a finite-dimensional space $X_h \subset X$ of (possibly very large) dimension $\dim(X_h) = N_h$. Hence, the full-order model (FOM) related to the forward problem reads as follows: given $\boldsymbol{\mu} \in \mathcal{P}$, find $u_h(\boldsymbol{\mu}) \in X_h$ such that

$$\begin{cases} a(u_h(\boldsymbol{\mu}), v_h; \boldsymbol{\mu}) = f(v_h; \boldsymbol{\mu}) & \forall v_h \in X_h & \text{(FOM state),} \\ \mathbf{s}_h(\boldsymbol{\mu}) = \boldsymbol{\ell}(u_h(\boldsymbol{\mu})) & & \text{(FOM observation).} \end{cases} \quad (2)$$

Under the above assumptions, problem (2) is well-posed and admits a unique solution for any $\boldsymbol{\mu} \in \mathcal{P}$. In particular, the following continuous dependence on data estimate holds:

$$\|u_h(\boldsymbol{\mu})\|_X \leq \frac{\|f(\cdot; \boldsymbol{\mu})\|_{X'}}{\alpha_h(\boldsymbol{\mu})} \quad \forall \boldsymbol{\mu} \in \mathcal{P}$$

being $\alpha_h(\boldsymbol{\mu})$ the (discrete) stability factor related to the PDE operator, that is

$$\alpha_h(\boldsymbol{\mu}) = \inf_{v_h \in X_h} \frac{a(v_h, v_h; \boldsymbol{\mu})}{\|v_h\|_X^2} \geq \alpha_0 > 0 \quad \forall \boldsymbol{\mu} \in \mathcal{P},$$

for a suitable $\alpha_0 \in \mathbb{R}$. Being able to efficiently evaluate a tight lower bound $0 < \alpha_h^{LB}(\boldsymbol{\mu}) \leq \alpha_h(\boldsymbol{\mu})$ of the stability factor for any $\boldsymbol{\mu} \in \mathcal{P}$ plays a key role in the a posteriori error bounds related to the RB approximation and, finally, in the solution of the inverse problem.

If the forward problem consists of solving (2) to predict the outcome of an experiment – by computing $u(\boldsymbol{\mu})$ and evaluating the output $\mathbf{s}(\boldsymbol{\mu})$ – in an inverse problem observed data or measurements \mathbf{s}^* are used to estimate unknown parameters $\boldsymbol{\mu}$ characterizing the physical system. Such a problem can be cast in the optimal control framework, see e.g. [19] for further details. If \mathbf{s}^* is an experimental measure, possibly polluted by measurement error, we need to rely instead on a statistical framework in order to quantify uncertainties (due to both measurement errors and nuisance parameters) on the estimated parameter values.

2.2 Bayesian framework

We consider a Bayesian framework [17, 36, 37] for the solution of the inverse UQ problems. We model both the observations \mathbf{s}^* and the parameters $\boldsymbol{\mu}$ as random variables, by introducing suitable probability density functions (PDFs). The solution of the inverse problem is given by a point or interval estimation computed on the basis of the *posterior probability* density $\pi_{post} : \mathcal{P} \times Y \rightarrow \mathbb{R}_0^+$, i.e. the probability density of the parameter $\boldsymbol{\mu}$ given the measured value of \mathbf{s}^* , which can be obtained as

$$\pi_{post}(\boldsymbol{\mu} | \mathbf{s}^*) = \frac{\pi(\mathbf{s}^* | \boldsymbol{\mu}) \pi_{prior}(\boldsymbol{\mu})}{\eta(\mathbf{s}^*)} \quad (3)$$

thanks to *Bayes' theorem*. Here $\pi_{prior} : \mathcal{P} \rightarrow \mathbb{R}_0^+$ is the *prior probability* density, expressing all available information on $\boldsymbol{\mu}$ independently of the measurements on \mathbf{s}^* that will be considered as data; $\pi : Y \times \mathcal{P} \rightarrow \mathbb{R}_0^+$ is the *likelihood* function of \mathbf{s}^* conditionally to $\boldsymbol{\mu}$; finally

$$\eta(\mathbf{s}^*) = \int_{\mathcal{P}} \pi(\mathbf{s}^* | \boldsymbol{\mu}) \pi_{prior}(\boldsymbol{\mu}).$$

In order to describe measurement errors, we consider an *additive noise* model, that is, if we suppose that $\boldsymbol{\mu}$ is the true parameter, the outcome of the experiment is

$$\mathbf{s}^* = \mathbf{s}_h(\boldsymbol{\mu}) + \boldsymbol{\varepsilon}_{noise} = \boldsymbol{\ell}(u_h(\boldsymbol{\mu})) + \boldsymbol{\varepsilon}_{noise}, \quad (4)$$

where the measurement noise $\boldsymbol{\varepsilon}_{noise}$ follows a probability distribution π_{noise} .

In this way, our data are d noisy s -variate measures $\{\mathbf{s}_1^*, \dots, \mathbf{s}_d^*\}$, $\mathbf{s}_i^* \in \mathbb{R}^s$ for any $i = 1, \dots, d$, modelled by assuming that the outcome of the numerical model is given by the output evaluated for the *true* parameter value. The most typical description of experimental uncertainties is the Gaussian model, that is, we deal with normally distributed, uncorrelated errors $\varepsilon_{\text{noise}} \sim \mathcal{N}(\mathbf{0}, \sigma_i^2 \delta_{ij})$, $i, j = 1, \dots, s$, with known variances σ_i^2 , independent of $\boldsymbol{\mu}$. We also denote the likelihood function appearing in (3) by highlighting the dependence on the FE space, as

$$\pi(\mathbf{s}^* | \boldsymbol{\mu}) = \pi^h(\mathbf{s}^* | \boldsymbol{\mu}) = \pi_\varepsilon(\mathbf{s}^* - \mathbf{s}_h(\boldsymbol{\mu})) \quad (5)$$

so that the expression of the posterior PDF given by (3) is as follows:

$$\pi_{post}^h(\boldsymbol{\mu} | \mathbf{s}^*) = \frac{\pi^h(\mathbf{s}^* | \boldsymbol{\mu}) \pi_{prior}(\boldsymbol{\mu})}{\eta_h(\mathbf{s}^*)}, \quad \text{being} \quad \eta_h(\mathbf{s}^*) = \int_{\mathcal{P}} \pi^h(\mathbf{s}^* | \boldsymbol{\mu}) \pi_{prior}(\boldsymbol{\mu}). \quad (6)$$

We highlight the dependence of the FE space on the posterior PDF, too. If the output depends linearly on the parameters and we choose a Gaussian prior, the posterior is also Gaussian. Instead, as soon as $\boldsymbol{\mu} \mapsto \mathbf{s}(\boldsymbol{\mu})$ is a nonlinear map, the expression of the likelihood function yields a posterior distribution which cannot be written in closed form, requiring instead an exhaustive exploration of the parameter space. This becomes very hard to perform, above all if the parameter space has a large dimension. We then need to rely on Monte Carlo Markov Chain (MCMC) to sample the posterior PDF, such as the well-known Metropolis-Hastings or Gibbs sampling techniques [14, 22]. These methods are exploited to draw a sequence of random samples from a (multi-dimensional) PDF which cannot be expressed in closed form. This is meant in order not only to approximate the posterior PDF, but also to compute integrals related to this distribution. Then, since we are not interested in the nuisance parameters $\boldsymbol{\zeta}$, we proceed to marginalize them. This leads to computing the conditional marginal distribution

$$\pi_{post}^h(\boldsymbol{\gamma} | \mathbf{s}^*) = \frac{1}{\eta_h(\mathbf{s}^*)} \int_{\mathcal{P}_\zeta} \pi^h(\mathbf{s}^* | \boldsymbol{\mu}) \pi_{prior}(\boldsymbol{\gamma}, \boldsymbol{\zeta}) d\boldsymbol{\zeta}. \quad (7)$$

MCMC methods are needed to evaluate (possibly) high-dimensional integrals like the one in (7). These methods involve repeated evaluations of the likelihood function $\pi^h(\mathbf{s}^* | \boldsymbol{\gamma}, \boldsymbol{\zeta})$ – and thus repeated evaluations of the forward problem (2) – so that relying on the FOM would be too expensive also in the case of linear elliptic problems.

Therefore, we seek to replace (2) with a computationally less expensive, reduced-order model providing an inexpensive approximation $u_n(\boldsymbol{\mu})$ to $u_h(\boldsymbol{\mu})$. This allows to compute a reduced-order (and inexpensive) approximation $\mathbf{s}_n(\boldsymbol{\mu})$ to the full-order output $\mathbf{s}_h(\boldsymbol{\mu})$. Replacing the *truth*, full-order likelihood function π^h with its ROM approximation

$$\pi^n(\mathbf{s}^* | \boldsymbol{\mu}) = \pi_\varepsilon(\mathbf{s}^* - \mathbf{s}_n(\boldsymbol{\mu})) \quad (8)$$

clearly affects the posterior distribution, which changes as follows:

$$\pi_{post}^n(\boldsymbol{\mu} | \mathbf{s}^*) = \frac{\pi^n(\mathbf{s}^* | \boldsymbol{\mu}) \pi_{prior}(\boldsymbol{\mu})}{\eta_n(\mathbf{s}^*)}, \quad \text{being} \quad \eta_n(\mathbf{s}^*) = \int_{\mathcal{P}} \pi^n(\mathbf{s}^* | \boldsymbol{\mu}) \pi_{prior}(\boldsymbol{\mu}). \quad (9)$$

Consequently, the marginal PDF of the identifiable parameters becomes

$$\pi_{post}^n(\boldsymbol{\gamma} | \mathbf{s}^*) = \frac{1}{\eta_n(\mathbf{s}^*)} \int_{\mathcal{P}_\zeta} \pi^n(\mathbf{s}^* | \boldsymbol{\mu}) \pi_{prior}(\boldsymbol{\gamma}, \boldsymbol{\zeta}) d\boldsymbol{\zeta}. \quad (10)$$

Nevertheless, being able to quantify the ROM effect on the inversion procedure by relying on a suitable measure of the error $\mathbf{s}_h(\boldsymbol{\mu}) - \mathbf{s}_n(\boldsymbol{\mu})$ is paramount: the main goal of this paper is to set up a suitable procedure to answer this question.

3 Reduced order models and a posteriori error bounds

Solving large PDE systems for several parameter values may require huge computational resources, unless efficient and reliable ROMs for parametrized PDEs are used. Here we recall the basic ingredients of these techniques and a posteriori error bounds, which are both crucial for the speed up of inverse UQ problems.

3.1 Reduced subspaces and projection-based ROMs

In this paper we consider a projection-based ROM, that is, an efficient way to compute an approximation $u_n(\boldsymbol{\mu})$ of the solution $u_h(\boldsymbol{\mu})$ (as well as an approximation $\mathbf{s}_n(\boldsymbol{\mu})$ of the output $\mathbf{s}_h(\boldsymbol{\mu})$) through a Galerkin projection onto a reduced subspace X_n ; given $\boldsymbol{\mu} \in \mathcal{P}$, find $u_n(\boldsymbol{\mu}) \in X_n$ s.t.

$$\begin{cases} a(u_n(\boldsymbol{\mu}), v_n; \boldsymbol{\mu}) = f(v_n; \boldsymbol{\mu}) & \forall v_n \in X_n & \text{(ROM state)} \\ \mathbf{s}_n(\boldsymbol{\mu}) = \boldsymbol{\ell}(u_n(\boldsymbol{\mu})) & & \text{(ROM observation),} \end{cases} \quad (11)$$

where $\dim(X_n) = n \ll N_h$. The reduced subspace X_n is constructed from a set of (well-chosen) full-order solutions, usually by exploiting one of the following techniques [20, 33]:

- *greedy reduced basis.* Basis functions are obtained by orthonormalizing a set of full-order solutions, corresponding to a specific choice $S_n = \{\boldsymbol{\mu}^1, \dots, \boldsymbol{\mu}^n\}$ of parameter values, built by means of the following *greedy* procedure. Let us denote $\Xi_{train} \subset \mathcal{P}$ a (sufficiently rich) finite training sample, selected from \mathcal{P} according to a uniform distribution. Given a prescribed $\boldsymbol{\mu}^1 \in \Xi_{train}$ and a sharp, inexpensive error bound $\Delta_n(\boldsymbol{\mu})$ (see Section 3.3) such that

$$\|u_h(\boldsymbol{\mu}) - u_n(\boldsymbol{\mu})\|_X \leq \Delta_n(\boldsymbol{\mu}) \quad \text{for all } \boldsymbol{\mu} \in \mathcal{P},$$

we choose the remaining parameter values as

$$\boldsymbol{\mu}^n := \arg \max_{\boldsymbol{\mu} \in \Xi_{train}} \Delta_{n-1}(\boldsymbol{\mu}), \quad \text{for } n = 2, \dots, n_{max}$$

until $\Delta_{n_{max}}(\boldsymbol{\mu}) \leq \varepsilon_{tol}^{RB}$ for all $\boldsymbol{\mu} \in \Xi_{train}$, being ε_{tol}^{RB} a suitably small tolerance.

- *proper orthogonal decomposition.* In this case, the reduced subspace X_n is given by the first n (left) singular vectors of the snapshot matrix $S = [u_h(\boldsymbol{\mu}^1) \mid \dots \mid u_h(\boldsymbol{\mu}^{N_s})] \in \mathbb{R}^{N_h \times N_s}$, corresponding to the largest n singular values $\sigma_1 \geq \sigma_2 \geq \dots \geq \sigma_n$. Here $u_h(\boldsymbol{\mu}^1), \dots, u_h(\boldsymbol{\mu}^{N_s})$ are N_s high-fidelity solutions of the forward problem, computed for a random sample $\boldsymbol{\mu}^1, \dots, \boldsymbol{\mu}^{N_s}$. By construction, the POD basis is orthonormal; moreover, the error in the basis is equal to the squares of the singular values corresponding to the neglected modes, and the maximum subspace dimension is such that

$$\sum_{i=n+1}^r \sigma_i^2 \leq \varepsilon_{tol}^{POD} \quad r = \min\{N_s, N_h\},$$

being ε_{tol}^{POD} a suitably small tolerance.

3.2 Affine parametric dependence and Offline/Online decomposition

Constructing the reduced subspace requires several evaluation of the FOM, which are performed only once, during the so-called *Offline* stage. Each *Online* evaluation of the reduced solution (and related output) requires to solve a problem of very small dimension $n \ll N_h$. Such an Offline/Online decomposition is made possible under the assumption that a suitable *affine parametric dependence* property is fulfilled by the $\boldsymbol{\mu}$ -dependent operators. Hence, we require that $a(\cdot, \cdot; \boldsymbol{\mu})$, $f(\cdot; \boldsymbol{\mu})$ can be written as a separable expansion of $\boldsymbol{\mu}$ -independent bilinear/linear forms:

$$a(u, v; \boldsymbol{\mu}) = \sum_{q=1}^{Q_a} \Theta_q^a(\boldsymbol{\mu}) a_q(u, v), \quad f(v; \boldsymbol{\mu}) = \sum_{q=1}^{Q_f} \Theta_q^f(\boldsymbol{\mu}) f_q(v)$$

for some integers Q_a, Q_f . A similar decomposition would be required also on the linear forms $\boldsymbol{\ell}^j$, $j = 1, \dots, s$, if they were $\boldsymbol{\mu}$ -dependent, too.

3.3 A posteriori error bounds

We can easily derive an *a posteriori* (residual-based) error bound w.r.t. the full-order solution, for both the PDE solution and related outputs [33], whenever dealing with linear equations and outputs. Let us denote by $r(w; \boldsymbol{\mu}) = f(w; \boldsymbol{\mu}) - a(u_n(\boldsymbol{\mu}), w; \boldsymbol{\mu})$, for any $w \in X_h$, the residual of the

state equation and its dual norm by $\|r(\cdot; \boldsymbol{\mu})\|_{X'} = \sup_{v \in X_h} \frac{r(v; \boldsymbol{\mu})}{\|v\|_X}$. Then, the error bound on the solution reads as follows:

$$\|u_h(\boldsymbol{\mu}) - u_n(\boldsymbol{\mu})\|_X \leq \Delta_n(\boldsymbol{\mu}) := \frac{\|r(\cdot; \boldsymbol{\mu})\|_{X'}}{\alpha_h^{LB}(\boldsymbol{\mu})} \quad \forall \boldsymbol{\mu} \in \mathcal{P}. \quad (12)$$

We remark that also the computation of the dual norm of residuals, as well as of the lower bound α_h^{LB} to the stability factors, takes advantage of a similar *Offline-Online* stratagem, allowing to get an inexpensive evaluation of the error bound for each $\boldsymbol{\mu} \in \mathcal{P}$; see e.g. [33].

Regarding the error bound on the output, which is relevant to the Bayesian inversion, we recall here its expression in the case of linear, *noncompliant* outputs, as the numerical test cases presented in the remainder deal with this situation. For any $\ell^j \in X'$, let us introduce the following (full-order approximation of the) *dual* problem: find $\psi_h^j(\boldsymbol{\mu}) \in X_h$ such that

$$a(v_h, \psi_h^j(\boldsymbol{\mu}); \boldsymbol{\mu}) = -\ell^j(v_h) \quad \forall v_h \in X_h.$$

In addition to the reduced space for the forward problem (2) (which can be referred to as the *primal* problem), let us define a reduced subspace for each dual problem, by using the same algorithm (either greedy-RB or POD) chosen for the primal problem. Here X_n^j denotes the dual subspace related to the j -th output, although the dimension of each of these subspaces can be different, and differ from n . The resulting RB approximation $\psi_n^j(\boldsymbol{\mu}) \in X_n^j$ solves

$$a(v_n, \psi_n^j(\boldsymbol{\mu}); \boldsymbol{\mu}) = -\ell^j(v_n) \quad \forall v_n \in X_n^j$$

and is required to get the following error bound on the output:

$$|s_h^j(\boldsymbol{\mu}) - s_n^j(\boldsymbol{\mu})| \leq \Delta_n^j(\boldsymbol{\mu}) \equiv \frac{\|r(\cdot; \boldsymbol{\mu})\|_{(X_h)'}}{(\alpha_h^{LB}(\boldsymbol{\mu}))^{1/2}} \frac{\|r^j(\cdot; \boldsymbol{\mu})\|_{(X_h)'}}{(\alpha_h^{LB}(\boldsymbol{\mu}))^{1/2}} \quad \forall \boldsymbol{\mu} \in \mathcal{P} \quad (13)$$

where $r^j(w; \boldsymbol{\mu}) = -\ell^j(w) - a(w, \psi_n^j(\boldsymbol{\mu}); \boldsymbol{\mu})$, $\forall w \in X_h$, is the dual residual related to the j -th output. Here $s_h^j(\boldsymbol{\mu}) = \ell^j(u_h(\boldsymbol{\mu}))$ denotes the full-order j -th output, whereas $s_n^j(\boldsymbol{\mu}) = \ell^j(u_n(\boldsymbol{\mu}))$ is the corresponding ROM output. In the same way, for the RB dual solution we have:

$$\|\psi_h^j(\boldsymbol{\mu}) - \psi_n^j(\boldsymbol{\mu})\|_X \leq \Delta_n^j(\boldsymbol{\mu}) := \frac{\|r^j(\cdot; \boldsymbol{\mu})\|_{X'}}{\alpha_h^{LB}(\boldsymbol{\mu})} \quad \forall \boldsymbol{\mu} \in \mathcal{P}.$$

As already remarked for the primal residuals, also dual residuals can be efficiently evaluated by taking advantage of the affine $\boldsymbol{\mu}$ -dependence. We also denote by

$$\Phi_n^j(\boldsymbol{\mu}) = \frac{\Delta_n^j(\boldsymbol{\mu})}{s_h^j(\boldsymbol{\mu}) - s_n^j(\boldsymbol{\mu})} \quad \forall \boldsymbol{\mu} \in \mathcal{P}, \quad 1 \leq j \leq s$$

the effectivity of the estimator $\Delta_n^j(\boldsymbol{\mu})$. It is possible to show that $1 \leq |\Phi_n^j(\boldsymbol{\mu})| \leq M_h(\boldsymbol{\mu})/\alpha_h^{LB}(\boldsymbol{\mu})$, where $M_h(\boldsymbol{\mu})$ is the FE continuity constant of $a(\cdot, \cdot; \boldsymbol{\mu})$, see e.g. [33] for further details.

4 Reduction Error Models

Being able to evaluate the output quantity of a PDE system at a greatly reduced cost is essential to speed up the solution of inverse UQ problems within a Bayesian framework. Our goal, once a RB approximation has been built in the offline stage, is to exploit its fast and inexpensive online queries to speed up the evaluation of the posterior PDF, of related (point or interval) estimates, and of MCMC integrals like (7) or (10). Not only, by taking into account reduction errors or available error bounds, we can obtain *reliable* solutions at the end of the inversion process, too. Although ROMs have been exploited to speed up the solution of inverse problems in several works, very few papers have focused on the analysis of reduction error propagation.

In particular, we wish to incorporate a model for the error engendered by the ROM into the Bayesian estimator. To this end, we provide suitable (both deterministic and statistical) *reduction error models* (REMs), possibly by exploiting available error bounds on the outcome of the forward problem.

A basic observation is made possible by expressing, when dealing with *linear* (w.r.t. the PDE solution) outputs, the measurement equation (4) as

$$\mathbf{s}^* = \boldsymbol{\ell}(u_n(\boldsymbol{\mu})) + [\boldsymbol{\ell}(u_h(\boldsymbol{\mu})) - \boldsymbol{\ell}(u_n(\boldsymbol{\mu}))] + \boldsymbol{\varepsilon}_{\text{noise}} = \boldsymbol{\ell}(u_n(\boldsymbol{\mu})) + \boldsymbol{\delta}(\boldsymbol{\mu}) \quad (14)$$

where $\boldsymbol{\delta}(\boldsymbol{\mu}) = \boldsymbol{\varepsilon}_{\text{ROM}}(\boldsymbol{\mu}) + \boldsymbol{\varepsilon}_{\text{noise}}$ and

$$\boldsymbol{\varepsilon}_{\text{ROM}}(\boldsymbol{\mu}) = [s_h^1(\boldsymbol{\mu}) - s_n^1(\boldsymbol{\mu}), \dots, s_h^s(\boldsymbol{\mu}) - s_n^s(\boldsymbol{\mu})]^T \quad (15)$$

is the *reduction error*, that is, the error due to ROM approximation of the forward problem and related output. Although in principle $\boldsymbol{\varepsilon}_{\text{ROM}}$ is deterministic, in practice its evaluation is out of reach since it would require, for any $\boldsymbol{\mu}$, the solution of the full-order model. Here we propose three approaches for approximating the reduction error $\boldsymbol{\varepsilon}_{\text{ROM}}(\boldsymbol{\mu})$ by a suitable indicator $\tilde{\boldsymbol{\varepsilon}}_{\#}(\boldsymbol{\mu})$, $\# = 1, 2, 3$, according to suitable reduction error models which can be easily incorporated in the Bayesian framework. In particular:

- in **[REM-1]** we treat ROM errors as *epistemic* uncertainties, represented through random variables, following the so-called *approximation error model* [1];
- in **[REM-2]** we provide a deterministic approximation of ROM errors by considering *radial basis* interpolants of the error over the parameter space;
- in **[REM-3]** we express ROM errors through a linear model depending on output error bounds, fitted through regression analysis.

Hence, we end up with error indicators which can be either deterministic – that is, $\tilde{\boldsymbol{\varepsilon}}(\boldsymbol{\mu}) = \mathbf{m}_{\text{ROM}}(\boldsymbol{\mu})$, being $\mathbf{m}_{\text{ROM}}(\boldsymbol{\mu})$ a suitable function of $\boldsymbol{\mu}$ – or expressed through a random variable $\tilde{\boldsymbol{\varepsilon}}(\boldsymbol{\mu})$, whose distribution $\pi_{\tilde{\boldsymbol{\varepsilon}}}$ is characterized by $\mathbf{m}_{\text{ROM}}(\boldsymbol{\mu}) = \mathbb{E}[\tilde{\boldsymbol{\varepsilon}}(\boldsymbol{\mu})]$ and $\Sigma_{\text{ROM}}(\boldsymbol{\mu}) = \text{Cov}[\tilde{\boldsymbol{\varepsilon}}(\boldsymbol{\mu})]$. Correspondingly, we end up with a *corrected* reduced-order likelihood

$$\tilde{\pi}^n(\mathbf{s}^* | \boldsymbol{\mu}) = \begin{cases} \pi_{\boldsymbol{\varepsilon}}(\mathbf{s}^* - \mathbf{s}_n(\boldsymbol{\mu}) - \mathbf{m}_{\text{ROM}}(\boldsymbol{\mu})) & \text{deterministic REM} \\ \pi_{\tilde{\boldsymbol{\delta}}}(\mathbf{s}^* - \mathbf{s}_n(\boldsymbol{\mu}) - \mathbf{m}_{\text{ROM}}(\boldsymbol{\mu})) & \text{statistical REM} \end{cases} \quad (16)$$

being $\tilde{\boldsymbol{\delta}}(\boldsymbol{\mu}) = \tilde{\boldsymbol{\varepsilon}}(\boldsymbol{\mu}) + \boldsymbol{\varepsilon}_{\text{noise}}$ and $\text{Cov}[\tilde{\boldsymbol{\delta}}(\boldsymbol{\mu})] = \Sigma_{\text{noise}}(\boldsymbol{\mu}) + \Sigma_{\text{ROM}}(\boldsymbol{\mu})$, by assuming that ROM errors and measurement noise are independent. Correspondingly, we obtain the following *corrected* reduced-order posterior PDF

$$\tilde{\pi}_{\text{post}}^n(\boldsymbol{\mu} | \mathbf{s}^*) = \frac{\tilde{\pi}^n(\mathbf{s}^* | \boldsymbol{\mu}) \pi_{\text{prior}}(\boldsymbol{\mu})}{\tilde{\eta}_n(\mathbf{s}^*)}, \quad \text{being} \quad \tilde{\eta}_n(\mathbf{s}^*) = \int_{\mathcal{P}} \tilde{\pi}^n(\mathbf{s}^* | \boldsymbol{\mu}) \pi_{\text{prior}}(\boldsymbol{\mu}), \quad (17)$$

yielding to a similar correction in the marginal PDF of the identifiable parameters (10). In the following subsections we discuss the construction of these three REMs.

4.1 REM-1: approximation error model

Following the so-called *approximation error model* of Kaipio et al. [1], we assume that ROM errors are the outcome of a Gaussian random variable, so that $\boldsymbol{\varepsilon}_{\text{ROM}}(\boldsymbol{\mu})$ is replaced by

$$\tilde{\boldsymbol{\varepsilon}}_1(\boldsymbol{\mu}) \sim \mathcal{N}(\mathbf{m}_{\text{ROM}}, \Sigma_{\text{ROM}}) \quad (18)$$

being $\mathbf{m}_{\text{ROM}} \in \mathbb{R}^s$ and $\Sigma_{\text{ROM}} \in \mathbb{R}^{s \times s}$ the sample constant mean and covariance, respectively, obtained by sampling N_{cal} errors $\{\mathbf{s}_h(\boldsymbol{\mu}^k) - \mathbf{s}_n(\boldsymbol{\mu}^k)\}_{k=1}^{N_{\text{cal}}}$:

$$\mathbf{m}_{\text{ROM}} = \frac{1}{N_{\text{cal}}} \sum_{k=1}^{N_{\text{cal}}} \boldsymbol{\varepsilon}_{\text{ROM}}(\boldsymbol{\mu}^k), \quad \Sigma_{\text{ROM}} = \frac{1}{N_{\text{cal}} - 1} \sum_{k=1}^{N_{\text{cal}}} (\boldsymbol{\varepsilon}_{\text{ROM}}(\boldsymbol{\mu}^k) - \mathbf{m}_{\text{ROM}})(\boldsymbol{\varepsilon}_{\text{ROM}}(\boldsymbol{\mu}^k) - \mathbf{m}_{\text{ROM}})^T.$$

We refer to the random sample $S_{N_{\text{cal}}} = \{\boldsymbol{\mu}^1, \dots, \boldsymbol{\mu}^{N_{\text{cal}}}\}$ as the *calibration set*, since the computational experiments leading to $\boldsymbol{\varepsilon}_{\text{ROM}}(\boldsymbol{\mu}^k)$, $\boldsymbol{\mu}^k \in S_{N_{\text{cal}}}$, are additional queries to both the FOM and the ROM, required to characterize our REM-1. In this case, the correction does not depend on $\boldsymbol{\mu}$ by construction. If we assume in addition that measurement errors are Gaussian – that is, $\boldsymbol{\varepsilon}_{\text{noise}} \sim \mathcal{N}(\mathbf{0}, \Sigma_{\text{noise}})$ – and independent from ROM errors, we have that

$$\tilde{\boldsymbol{\delta}}_1(\boldsymbol{\mu}) := \boldsymbol{\varepsilon}_{\text{noise}} + \tilde{\boldsymbol{\varepsilon}}_1(\boldsymbol{\mu}) \sim \mathcal{N}(\mathbf{m}_{\text{ROM}}, \Sigma_{\text{noise}} + \Sigma_{\text{ROM}}). \quad (19)$$

Indeed, the effect of the ROM error results in a *shift* of the likelihood function and an additional contribution to its variance, provided the normality assumption on the errors evaluated over $S_{N_{cal}}$ is fulfilled. In this case, only a slight modification of the numerical solver is required within the MCMC process, thus making this REM particularly easy to implement. Nevertheless, very often ROM errors do not show a Gaussian distribution, so that further operations are required in order to use such a REM.

To overcome this fact, we can generalize the previous framework by considering any (parametric) distribution for the ROM errors conveniently fitted on the set of calibration experiments, that is, $\tilde{\epsilon}_1(\boldsymbol{\mu}) \sim \pi_{\tilde{\epsilon}}(\boldsymbol{\mu})$ possibly depending on a set of shape parameters. Although we assume that ROM errors are independent from (Gaussian) measurement errors, the distribution of $\tilde{\delta}_1(\boldsymbol{\mu}) = \epsilon_{\text{noise}} + \tilde{\epsilon}_1(\boldsymbol{\mu})$ cannot be found, in general, in a closed form².

Thus, in the case of REM-1, a *global* approximation of the ROM error over the parameter space is provided – hence, not depending on $\boldsymbol{\mu}$ – by prescribing the distribution of a random variable fitted over a sample of *calibration experiments*.

4.2 REM-2: radial basis interpolation

Despite being straightforward, REM-1 can perform badly, for instance when ROM errors can not be explained by means of a sample statistical distributions in closed form, because of their complex variability over the parameter space. For this reason, we turn instead to a local error model, still exploiting the errors $\{\mathbf{s}_h(\boldsymbol{\mu}^k) - \mathbf{s}_n(\boldsymbol{\mu}^k)\}_{k=1}^{N_{cal}}$ computed over a calibration set $S_{N_{cal}}$, by considering a radial basis interpolant for each output component. In particular, a deterministic $\boldsymbol{\mu}$ -dependent correction can be obtained as

$$s_h^j(\boldsymbol{\mu}) - s_n^j(\boldsymbol{\mu}) \simeq \Pi^j(\boldsymbol{\mu}) \Delta_n^j(\boldsymbol{\mu}), \quad j = 1, \dots, s,$$

where $\Pi^j(\boldsymbol{\mu})$ is a weighted combination of radial basis functions (RBF), i.e.

$$\Pi^j(\boldsymbol{\mu}) = \sum_{k=1}^{N_{cal}} w_k \phi(\|\boldsymbol{\mu} - \boldsymbol{\mu}^k\|), \quad j = 1, \dots, s,$$

and the coefficients $\{w_k\}_{k=1}^{N_{cal}}$ are determined so that Π^j fulfills the following interpolation constraints over the calibration set:

$$\frac{s_h^j(\boldsymbol{\mu}^k) - s_n^j(\boldsymbol{\mu}^k)}{\Delta_n^j(\boldsymbol{\mu}^k)} = \Pi^j(\boldsymbol{\mu}^k), \quad k = 1, \dots, N_{cal}, \quad j = 1, \dots, s.$$

In other words, we compute an interpolant of the inverse³ effectivities $(\Phi_n^j(\boldsymbol{\mu}))^{-1} \in [-1, 1]$, for each $j = 1, \dots, s$. While $\phi : \mathbb{R}_0^+ \rightarrow \mathbb{R}$ is a fixed shape function, radial with respect to the Euclidean distance $\|\cdot\|$ over \mathbb{R}^p . Here we use multiquadric basis functions ($\phi(r) = \sqrt{1+r^2}$), see e.g. [6] for other available options. Thus, in our deterministic REM-2 we replace ROM errors $\epsilon_{\text{ROM}}(\boldsymbol{\mu})$ by $\tilde{\epsilon}_2(\boldsymbol{\mu})$, with

$$\mathbf{m}_{\text{ROM}}(\boldsymbol{\mu}) = [\Pi^1(\boldsymbol{\mu}) \Delta_n^1(\boldsymbol{\mu}), \dots, \Pi^s(\boldsymbol{\mu}) \Delta_n^s(\boldsymbol{\mu})]^T, \quad (21)$$

which features a $\boldsymbol{\mu}$ -dependent shifting of the likelihood function. If in addition we want to take into account the variability of the ROM errors, we can incorporate the sample covariance evaluated over the calibration set as in REM-1, and thus consider⁴

$$\tilde{\delta}_2(\boldsymbol{\mu}) := \epsilon_{\text{noise}} + \tilde{\epsilon}_2(\boldsymbol{\mu}) \sim \mathcal{N}(\mathbf{m}_{\text{ROM}}(\boldsymbol{\mu}), \Sigma_{\text{noise}} + \Sigma_{\text{ROM}}(\boldsymbol{\mu})).$$

²In these cases, at each step of the MCMC process, we quantify $\tilde{\delta}_1(\boldsymbol{\mu})$ by calculating the realization of the sum of two random variables. One possible strategy is to calculate the following convolution:

$$\tilde{\delta}_1(\boldsymbol{\mu}) = \int_{\mathcal{P}} \pi_{\tilde{\epsilon}}(\boldsymbol{\mu} + \boldsymbol{\nu}) \pi_{\epsilon}(\boldsymbol{\nu}) d\boldsymbol{\nu}. \quad (20)$$

The evaluation of this integral can be performed, e.g., by an internal MCMC algorithm, which does not feature expensive extra calculations at each step of the outer MCMC process.

³This choice yields more accurate results than those obtained by interpolating ROM errors over the calibration set, that is, by considering $s_h^j(\boldsymbol{\mu}^k) - s_n^j(\boldsymbol{\mu}^k) = \tilde{\Pi}^j(\boldsymbol{\mu}^k)$, $k = 1, \dots, N_{cal}$, $j = 1, \dots, s$ (see Sect. 7.1).

⁴Assuming that ROM errors are Gaussian might be very limiting, as highlighted in the previous section. Here we consider this argument just as an heuristic correction.

Although very simple to be characterized, REM-2 suffers from the usual *curse of dimensionality*, so that both sampling the parameter space and evaluating calibration experiments becomes less and less affordable for increasing $p = \dim(\mathcal{P})$. Nevertheless, RBF interpolation is suitable for scattered data and, for the cases at hand, shows a very good compromise between accuracy and simplicity.

4.3 REM-3: linear regression model

A possible way to overcome the curse of dimensionality is to rely on a model where the *surrogate* ROM error is computed as a function of a scalar quantity depending on $\boldsymbol{\mu}$, rather than on $\boldsymbol{\mu}$ itself, no matter which is the parametric dimension p of $\boldsymbol{\mu} \in \mathcal{P} \subset \mathbb{R}^p$. In fact, the quantity which provides a good, inexpensive and readily available representation of the ROM error is the a posteriori error bound (13).

In order to derive a REM depending on a posteriori error bounds, we remark that a linear dependence between (the absolute values of the) output errors and related error bounds is shown when considering a *logarithmic* transformation, as already pointed out in a recent contribution [10]. Thus, we can in principle consider the following model:

$$\ln |s_h^j(\boldsymbol{\mu}) - s_n^j(\boldsymbol{\mu})| = \beta_0^j + \beta_1^j \ln(\Delta_n^j(\boldsymbol{\mu})) + \delta_{reg}^j, \quad j = 1, \dots, s \quad (22)$$

being $\delta_{reg}^j \sim \mathcal{N}(0, \sigma_{reg,j}^2)$, and fit it to the datasets $\{\Delta_n^j(\boldsymbol{\mu}^k), s_h^j(\boldsymbol{\mu}^k) - s_n^j(\boldsymbol{\mu}^k)\}_{k=1}^{N_{cal}}$ obtained by sampling errors and corresponding error bounds for each output, over a calibration set $S_{N_{cal}}$. By doing this, we get the estimates $\hat{\beta}_0^j, \hat{\beta}_1^j$ of the coefficients by exploiting standard linear regression theory, as well as the estimate of the variances $\hat{\sigma}_{reg,j}^2$ through the corresponding mean square errors. Thus, by fitting model (22) we obtain the following relation for the absolute value of the ROM error:

$$|s_h^j(\boldsymbol{\mu}) - s_n^j(\boldsymbol{\mu})| = \exp(\hat{\beta}_0^j + \hat{\beta}_1^j \ln(\Delta_n^j(\boldsymbol{\mu})) + \hat{\delta}_{reg}^j), \quad j = 1, \dots, s$$

being $\hat{\delta}_{reg}^j \sim \mathcal{N}(0, \hat{\sigma}_{\delta,j}^2)$. If we consider the deterministic REM-3, the absolute value of ROM errors $|\boldsymbol{\varepsilon}_{ROM}(\boldsymbol{\mu})|$ can be replaced by

$$\mathbf{m}_{ROM}(\boldsymbol{\mu}) = \left[\exp\left(\hat{\beta}_0^1 + \hat{\beta}_1^1 \ln(\Delta_n^1(\boldsymbol{\mu}))\right), \dots, \exp\left(\hat{\beta}_0^s + \hat{\beta}_1^s \ln(\Delta_n^s(\boldsymbol{\mu}))\right) \right]^T. \quad (23)$$

Instead, by taking into account the variability shown by ROM errors, $|\boldsymbol{\varepsilon}_{ROM}(\boldsymbol{\mu})|$ would be replaced by the following log-normal random variables:

$$\tilde{\boldsymbol{\varepsilon}}_3(\boldsymbol{\mu}) \sim \left[\log\mathcal{N}(\hat{\beta}_0^1 + \hat{\beta}_1^1 \ln(\Delta_n^1(\boldsymbol{\mu})), \hat{\sigma}_{reg,1}^2(\boldsymbol{\mu})), \dots, \log\mathcal{N}(\hat{\beta}_0^s + \hat{\beta}_1^s \ln(\Delta_n^s(\boldsymbol{\mu})), \hat{\sigma}_{reg,s}^2(\boldsymbol{\mu})) \right]^T. \quad (24)$$

However, in both cases no indications about the *sign* of the error are provided by the error bound (13), so that a correction based on (22) would be necessarily too poor. Once we have fitted the linear models, we shall infer the error sign (on each output component $j = 1, \dots, s$) from the calibration set, in order to replace $\tilde{\boldsymbol{\varepsilon}}_{ROM}^j(\boldsymbol{\mu})$ by $\rho_j \tilde{\boldsymbol{\varepsilon}}_3^j(\boldsymbol{\mu})$, where $\tilde{\boldsymbol{\varepsilon}}_3^j(\boldsymbol{\mu})$ is given by (23) or (24) and $\rho_j \in \{-1, +1\}$ is determined by adopting one of the following strategies:

1. *nearest neighbor*, assigning to $\tilde{\boldsymbol{\varepsilon}}_3^j(\boldsymbol{\mu})$ the sign of the sampled error in the calibration set closest to $\boldsymbol{\mu}$, that is

$$\rho_j = \text{sgn}\left(s_h^j(\hat{\boldsymbol{\mu}}^k) - s_n^j(\hat{\boldsymbol{\mu}}^k)\right), \quad \hat{\boldsymbol{\mu}}^k = \arg \min_{\boldsymbol{\mu}^k \in S_{N_{cal}}} \|\boldsymbol{\mu} - \boldsymbol{\mu}^k\|;$$

2. *Bernoulli trial*, assigning to $\tilde{\boldsymbol{\varepsilon}}_3^j(\boldsymbol{\mu})$ the sign:

$$\rho_j = -1 + 2X_j, \quad X_j \sim \mathcal{B}e(\hat{p}^j), \quad \hat{p}^j = \frac{|S_+^j|}{N_{cal}} \in [0, 1],$$

being $S_+^j = \{s_h^j(\boldsymbol{\mu}) - s_n^j(\boldsymbol{\mu}) > 0 : \boldsymbol{\mu} \in S_{N_{cal}}\}$ and $S_-^j = \{s_h^j(\boldsymbol{\mu}) - s_n^j(\boldsymbol{\mu}) < 0 : \boldsymbol{\mu} \in S_{N_{cal}}\}$.

The splitting of the calibration set in two subsets S_+^j and S_-^j suggests to consider a regression model over each subset, depending on the computed errors sign. In conclusion, we obtain for each $\boldsymbol{\mu} \in \mathcal{P}$ the random variable:

$$\tilde{\boldsymbol{\delta}}_3(\boldsymbol{\mu}) := \boldsymbol{\varepsilon}_{\text{noise}} + \boldsymbol{\rho} \tilde{\boldsymbol{\varepsilon}}_3(\boldsymbol{\mu}) \quad (25)$$

which is the sum of two random variables with different distributions (and can be computed similarly to (20)).

5 Inversion procedure

Let us now summarize the whole numerical procedure we use to solve a parametric inverse UQ problem. A first *offline* stage (Algorithm 1) consists in the computation of the reduced space and in the additional calibration set evaluation. During the *online* stage (Algorithm 2), a MCMC procedure is performed by considering at each iteration the reduced output $\mathbf{s}_n(\boldsymbol{\mu})$ instead of the full-order output $\mathbf{s}_h(\boldsymbol{\mu})$.

Algorithm 1 Offline procedure

- 1: **procedure** BASIS COMPUTATION
 - 2: *FE matrices:*
 - 3: $A_q^h, F_q^h \leftarrow \text{state problem}$
 - 4: $L_{q,s}^h \leftarrow \text{output evaluation \& dual problems}$
 - 5: *Lower bound:*
 - 6: $\alpha_{LB}(\boldsymbol{\mu}) \leftarrow \text{successive constraint method / heuristic strategies}$
 - 7: *Greedy procedure state problem:*
 - 8: **while** $\max_{i \in \Xi_{\text{train}}} \Delta_n(\boldsymbol{\mu}_i) > \varepsilon_{RB}^{\text{tol}}$ **do**
 - 9: $\boldsymbol{\mu}^n = \arg \max_{i \in \Xi_{\text{train}}} \Delta_n(\boldsymbol{\mu}_i); S_n = S_{n-1} \cup \text{span}\{u_h(\boldsymbol{\mu}^n)\}$
 - 10: $A_q^n, f_q^n \leftarrow \text{compute reduced state matrices}$
 - 11: *Greedy procedure dual problems: for each output $j = 1, \dots, s$*
 - 12: **while** $\max_{i \in \Xi_{\text{train}}} \Delta_n^j(\boldsymbol{\mu}_i) > \varepsilon_{RB}^{\text{tol}}$ **do**
 - 13: $\boldsymbol{\mu}_j^n = \arg \max_{i \in \Xi_{\text{train}}} \Delta_n^j(\boldsymbol{\mu}_i); S_n^j = S_{n-1}^j \cup \text{span}\{\psi_h^j(\boldsymbol{\mu}_j^n)\}$
 - 14: $A_{q,j}^n, L_{q,j}^n \leftarrow \text{compute reduced dual matrices}$
 - 15: **procedure** REM CALIBRATION
 - 16: **for** $j = 1 : N_{\text{cal}}$ **do**
 - 17: $\mathbf{s}_h(\boldsymbol{\mu}^j), u_h(\boldsymbol{\mu}^j) \leftarrow \text{FE state problem}$
 - 18: $\mathbf{s}_n(\boldsymbol{\mu}^j), u_n(\boldsymbol{\mu}^j), \Delta_n^{(1:s)}(\boldsymbol{\mu}^j) \leftarrow \text{RB state and dual problems}$
 - 19: $\text{err}_{j,1:s} = \mathbf{s}_h^{(1:s)}(\boldsymbol{\mu}^j) - \mathbf{s}_n^{(1:s)}(\boldsymbol{\mu}^j)$
 - 20: compute REM
-

The selection of the basis functions is performed through a *greedy (RB)* algorithm. This procedure requires the efficient evaluation of the a posteriori error bound (12), for which a suitable offline/online procedure is exploited (see [25] for further details). The calibration procedure consists in evaluating the difference between the ROM output $\mathbf{s}_n(\boldsymbol{\mu})$ and the full-order output $\mathbf{s}_h(\boldsymbol{\mu})$ for each parameter in the calibration set $S_{N_{\text{cal}}}$. Finally, the REM construction is performed accordingly to the procedure described in section 4.

During the *online* stage, the *posterior* distribution is sampled through a Metropolis–Hastings algorithm, which generates a sequence of sample values, whose distribution converges to the desired corrected distribution $\tilde{\pi}_{\text{post}}^n$. Each MCMC iteration entails an *online* query, which is performed in an efficient way by the ROM and the REM. The quality of the sampling sequence is finally improved by performing a subsequent *burn-in* and *thinning*, in order to reduce the autocorrelation between the sampled points; see e.g. [14, 22] for further details.

Algorithm 2 Online procedure

```

1: procedure METROPOLIS SAMPLING
2:    $\boldsymbol{\mu}^{(1)} \leftarrow$  initial value
3:   sampling loop:
4:   for cont = 2 : K do
5:      $\bar{\boldsymbol{\mu}} \leftarrow$  random walk
6:      $[\mathbf{s}_n(\bar{\boldsymbol{\mu}}), \Delta_n(\bar{\boldsymbol{\mu}})] \leftarrow$  compute RB state + dual problems
7:      $\mathbf{m}_{\text{ROM}}(\bar{\boldsymbol{\mu}}) \leftarrow$  evaluate REM mean
8:     if REM is deterministic then
9:        $\tilde{\pi}^n \leftarrow \pi_\varepsilon(\mathbf{s}^* - \mathbf{s}_n(\bar{\boldsymbol{\mu}}) - \mathbf{m}_{\text{ROM}}(\bar{\boldsymbol{\mu}}))$ 
10:    if REM is statistical then
11:       $\Sigma_{\text{ROM}}(\bar{\boldsymbol{\mu}}) \leftarrow$  evaluate REM covariance matrix
12:       $\tilde{\pi}^n \leftarrow \pi_{\tilde{\delta}}(\mathbf{s}^* - \mathbf{s}_n(\bar{\boldsymbol{\mu}}) - \mathbf{m}_{\text{ROM}}(\bar{\boldsymbol{\mu}}))$ 
13:       $\tilde{\pi}_{\text{post}}^n(\bar{\boldsymbol{\mu}}|\mathbf{s}^*) \leftarrow$  Bayes' formula
14:       $\gamma \leftarrow \tilde{\pi}_{\text{post}}^n(\bar{\boldsymbol{\mu}}|\mathbf{s}^*) / \tilde{\pi}_{\text{post}}^n(\boldsymbol{\mu}^{(k)}|\mathbf{s}^*)$ 
15:       $y \leftarrow$  random sampling from  $U(0, 1)$ 
16:      if  $y < \gamma$  then
17:         $\boldsymbol{\mu}^{(k+1)} \leftarrow \bar{\boldsymbol{\mu}}; k \leftarrow k + 1$ 
18:   burn-in:
19:     eliminate first M simulations  $\boldsymbol{\mu}^{(1:M)}$ 
20:   thinning:
21:     keep every d-th draw of the chain  $\boldsymbol{\mu}^{(1:d:\text{end})}$ 

```

6 Effectivity of proposed Reduction Error Models

Let us now analyze the effectivity of the *corrections* made on the reduced-order likelihood function thanks to the proposed reduction error models. In particular, we aim at stating some conditions to be fulfilled by REM corrections in order to guarantee that the corresponding posterior PDF $\tilde{\pi}_n$ is more robust and closer to the full-order PDF π_h than the reduced-order PDF π_n without corrections.

To this end, let us recall the notion of Kullback-Leibler (K-L) divergence, which is a non-symmetric measure of the difference between two probability distributions π_A and π_B , defined as

$$D_{KL}(\pi_A||\pi_B) = \int \pi_A(z) \log \left(\frac{\pi_A(z)}{\pi_B(z)} \right) dz. \quad (26)$$

Clearly, $D_{KL}(\pi_A||\pi_B) \geq 0$ whereas $D_{KL}(\pi_A||\pi_B) = 0$ if $\pi_A = \pi_B$ almost surely. This notion has already been used to compare approximations of posterior distributions obtained through generalized polynomial chaos representations, see e.g. [28, 5] for further details.

6.1 Consistency result

Before comparing our REMs and showing their effect on the reduced-order posterior PDFs, we prove that the reduced-order likelihood function π^n approximates the full-order one π^h in a *consistent* way, as long as the ROM dimension increases:

Proposition 1. *Let us consider the additive Gaussian noise model (4) and the RB approximation $s_n(\boldsymbol{\mu})$ of the output $s_h(\boldsymbol{\mu})$ defined by (11) and (2), by assuming an analytic $\boldsymbol{\mu}$ -dependence in the bilinear/linear forms. Then, for any $\boldsymbol{\mu} \in \mathcal{P}$,*

$$D_{KL}(\pi^h||\pi^n) = \sum_{j=1}^s \frac{1}{2\sigma_j^2} (s_h^j(\boldsymbol{\mu}) - s_n^j(\boldsymbol{\mu}))^2, \quad (27)$$

so that $\lim_{n \rightarrow N_h} D_{KL}(\pi^h||\pi^n) = 0$ exponentially.

Proof. The solution $u_n(\boldsymbol{\mu}) \in X_n$ of (2) is obtained as a Galerkin projection over X_n , then

$$\|u_h(\boldsymbol{\mu}) - u_n(\boldsymbol{\mu})\|_X \leq \left(\frac{\bar{M}}{\alpha_0}\right)^{1/2} \inf_{w_n \in X_n} \|u_h(\boldsymbol{\mu}) - w_n\|_X$$

being $M(\boldsymbol{\mu}) \leq \bar{M}$ the continuity constant of $a(\cdot, \cdot; \boldsymbol{\mu})$ and $\alpha_0 > 0$ such that $\alpha_h(\boldsymbol{\mu}) \geq \alpha_0$ for any $\boldsymbol{\mu} \in \mathcal{P}$. Thus we have that $\|u_h(\boldsymbol{\mu}) - u_n(\boldsymbol{\mu})\|_X \rightarrow 0$ when $n \rightarrow N_h$. By the same argument, $\|\psi_h(\boldsymbol{\mu}) - \psi_n(\boldsymbol{\mu})\|_X \rightarrow 0$ when $n \rightarrow N_h$. Moreover, the Kolmogorov n -width⁵ of the solution set \mathcal{M}_h converges exponentially:

$$d_n(\mathcal{M}_h; X) \leq C e^{-\alpha n} \quad \text{for some } C, \alpha > 0, \quad (28)$$

provided the $\boldsymbol{\mu}$ -dependence in the bilinear/linear forms is analytic; see [18] for further details. Regarding the output, by exploiting twice Galerkin orthogonality we have that

$$\begin{aligned} s_h^j(\boldsymbol{\mu}) - s_n^j(\boldsymbol{\mu}) &= l^j(u_h(\boldsymbol{\mu})) - l^j(u_n(\boldsymbol{\mu})) = a(u_n(\boldsymbol{\mu}), \psi_n(\boldsymbol{\mu}); \boldsymbol{\mu}) - a(u_h(\boldsymbol{\mu}), \psi_h(\boldsymbol{\mu}); \boldsymbol{\mu}) \\ &= a(u_n(\boldsymbol{\mu}) - u_h(\boldsymbol{\mu}), \psi_n(\boldsymbol{\mu}) - \psi_h(\boldsymbol{\mu}); \boldsymbol{\mu}). \end{aligned}$$

Then, $|s_h^j(\boldsymbol{\mu}) - s_n^j(\boldsymbol{\mu})| \leq \bar{M} \|u_h(\boldsymbol{\mu}) - u_n(\boldsymbol{\mu})\|_X \|\psi_h(\boldsymbol{\mu}) - \psi_n(\boldsymbol{\mu})\|_X$ so that, when $n \rightarrow N_h$, $|s_h^j(\boldsymbol{\mu}) - s_n^j(\boldsymbol{\mu})| \rightarrow 0$ for any $j = 1, \dots, s$; furthermore, the order of convergence of the ROM output to the FEM output is twice larger than the one of the state solution. In particular, by considering an additive Gaussian noise model, for any $\boldsymbol{\mu} \in \mathcal{P}$

$$D_{KL}(\pi^h || \pi^n) = \int_{\mathbb{R}^s} \pi^h(s | \boldsymbol{\mu}) \log \left(\frac{\pi^h(s | \boldsymbol{\mu})}{\pi^n(s | \boldsymbol{\mu})} \right) ds = \sum_{j=1}^s \frac{1}{2\sigma_j^2} (s_h^j(\boldsymbol{\mu}) - s_n^j(\boldsymbol{\mu}))^2,$$

thanks to the definition (26) of Kullback-Leibler divergence, so that $\lim_{n \rightarrow N_h} D_{KL}(\pi^h || \pi^n) \rightarrow 0$; finally, convergence takes place at exponential rate thanks to (28). \square

The consistency property can be extended to the posterior PDFs according to the

Proposition 2. *Under the assumptions of Proposition 1, $\lim_{n \rightarrow N_h} D_{KL}(\pi_{post}^h || \pi_{post}^n) \rightarrow 0$ exponentially.*

Proof. Thanks to the definition of K-L divergence,

$$\begin{aligned} D_{KL}(\pi_{post}^h || \pi_{post}^n) &= \int_{\mathcal{P}} \frac{\pi^h(\mathbf{s}^* | \boldsymbol{\mu}) \pi_{prior}(\boldsymbol{\mu})}{\eta_h(\mathbf{s}^*)} \log \left(\frac{\pi^h(\mathbf{s}^* | \boldsymbol{\mu}) \eta_n(\mathbf{s}^*)}{\pi^n(\mathbf{s}^* | \boldsymbol{\mu}) \eta_h(\mathbf{s}^*)} \right) d\boldsymbol{\mu} \\ &= \log \left(\frac{\eta_n(\mathbf{s}^*)}{\eta_h(\mathbf{s}^*)} \right) + \int_{\mathcal{P}} \frac{\pi^h(\mathbf{s}^* | \boldsymbol{\mu}) \pi_{prior}(\boldsymbol{\mu})}{\eta_h(\mathbf{s}^*)} \log \left(\frac{\pi^h(\mathbf{s}^* | \boldsymbol{\mu})}{\pi^n(\mathbf{s}^* | \boldsymbol{\mu})} \right) d\boldsymbol{\mu}. \end{aligned} \quad (29)$$

By using the definition of π^h and π^n , and the Lipschitz-continuity of $\exp(-\mathbf{s})$ for $\mathbf{s} \geq \mathbf{0}$ (that is, $|e^{-\mathbf{s}} - e^{-\mathbf{t}}| \leq \Lambda |\mathbf{s} - \mathbf{t}|$ for any $\mathbf{s}, \mathbf{t} > \mathbf{0}$, with $\Lambda = 1$), we obtain

$$\begin{aligned} |\pi^h(\mathbf{s}^* | \boldsymbol{\mu}) - \pi^n(\mathbf{s}^* | \boldsymbol{\mu})| &= \prod_{j=1}^s \frac{1}{\sqrt{2\pi\sigma_j^2}} \left| \exp \left(-\frac{(s_j^* - s_n^j(\boldsymbol{\mu}))^2}{2\sigma_j^2} \right) - \exp \left(-\frac{(s_j^* - s_h^j(\boldsymbol{\mu}))^2}{2\sigma_j^2} \right) \right| \\ &\leq \prod_{j=1}^s \frac{1}{\sqrt{2\pi\sigma_j^2}} \left| -\frac{(s_j^* - s_n^j(\boldsymbol{\mu}))^2}{2\sigma_j^2} + \frac{(s_j^* - s_h^j(\boldsymbol{\mu}))^2}{2\sigma_j^2} \right| \\ &\leq \prod_{j=1}^s \frac{1}{\sqrt{2\pi\sigma_j^2} 2\sigma_j^2} |s_n^j(\boldsymbol{\mu}) - s_h^j(\boldsymbol{\mu})| |2s_j^* - s_h^j(\boldsymbol{\mu}) - s_n^j(\boldsymbol{\mu})| \end{aligned}$$

so that, for any $\boldsymbol{\mu} \in \mathcal{P}$, $|\pi^h(\mathbf{s}^* | \boldsymbol{\mu}) - \pi^n(\mathbf{s}^* | \boldsymbol{\mu})| \rightarrow 0$ when $n \rightarrow N_h$ because $|s_h^j(\boldsymbol{\mu}) - s_n^j(\boldsymbol{\mu})| \rightarrow 0$ for any $j = 1, \dots, s$. In the same way, $|\eta_n(\mathbf{s}^*) - \eta_h(\mathbf{s}^*)| = \left| \int_{\mathcal{P}} (\pi^h(\mathbf{s}^* | \boldsymbol{\mu}) - \pi^n(\mathbf{s}^* | \boldsymbol{\mu})) \pi_{prior}(\boldsymbol{\mu}) d\boldsymbol{\mu} \right| \rightarrow 0$ for any given $\mathbf{s}^* \in \mathbb{R}^s$. Thus, both terms in the second line of (29) vanish for $n \rightarrow N_h$. \square

6.2 A result of effectivity for the proposed REMs

Since we are mainly interested in the case where the ROM dimension n is fixed (and possibly small) we want to show that performing a correction according to a REM improves the quality of the reduced posterior (in terms of the the K-L divergence).

⁵The Kolmogorov n -width $d_n(\mathcal{M}_h; X)$ measures how a finite dimensional subspace uniformly approximates the manifold $\mathcal{M}_h = \{u_h(\boldsymbol{\mu}), \boldsymbol{\mu} \in \mathcal{P}\}$ of the PDE solutions: $d_n(\mathcal{M}_h; X) = \inf_{X_n \subset X} \sup_{u_h \in \mathcal{M}_h} \inf_{w_n \in X_n} \|u_h - w_n\|_X$ where the first infimum is taken over all linear subspaces $X_n \subset X$ of dimension n .

By following the structure of the previous section, we first state a result dealing with the approximation of the likelihood function by a corrected ROM:

Proposition 3. *Under the same assumptions of Proposition 1, if there exists $C_j < 1$ such that, for any $j = 1, \dots, s$,*

$$|s_h^j(\boldsymbol{\mu}) - s_n^j(\boldsymbol{\mu}) - m_{ROM}^j(\boldsymbol{\mu})| \leq C_j |s_h^j(\boldsymbol{\mu}) - s_n^j(\boldsymbol{\mu})| \quad \forall \boldsymbol{\mu} \in \mathcal{P} \quad (30)$$

then

$$D_{KL}(\pi^h || \tilde{\pi}^n) \leq \left(\max_{j=1, \dots, s} C_j^2 \right) D_{KL}(\pi^h || \pi^n) \quad \forall \boldsymbol{\mu} \in \mathcal{P}. \quad (31)$$

provided that the correction is made according to a deterministic REM.

Proof. In analogy with relation (27), a correction operated by means of a deterministic REM affects just $\mathbb{E}[\mathbf{s}^* | \boldsymbol{\mu}]$, so that

$$D_{KL}(\pi^h || \tilde{\pi}^n) = \sum_{j=1}^s \frac{1}{2\sigma_j^2} (s_h^j(\boldsymbol{\mu}) - s_n^j(\boldsymbol{\mu}) - m_{ROM}^j(\boldsymbol{\mu}))^2. \quad (32)$$

Thus, under condition (30), (31) directly follows. \square

By means of (30), we require that the correction provided by a REM is *effective*, that is, it yields a reduction in the K-L divergence between the reduced-order and the high-fidelity posterior PDFs, when in the former case a correction through a deterministic REM is considered. Instead, when relying on statistical REMs, we need to distinguish between two cases:

- the correction shall result in a normal random variable (REM1 or REM2), with mean \mathbf{m}_{ROM} and covariance matrix $(\Sigma_{ROM})_{ij} = (\sigma_j^{ROM})^2 \delta_{ij}$. In this case, we would obtain

$$D_{KL}(\pi^h || \tilde{\pi}^n) = \frac{1}{2} \sum_{j=1}^s \left(\frac{(s_h^j(\boldsymbol{\mu}) - s_n^j(\boldsymbol{\mu}) - \bar{\varepsilon}^j(\boldsymbol{\mu}))^2}{\sigma_j^2 + (\sigma_j^{ROM})^2} + \frac{\sigma^2}{\sigma_j^2 + (\sigma_j^{ROM})^2} - 1 - \log \left(\frac{\sigma_j^2}{\sigma_j^2 + (\sigma_j^{ROM})^2} \right) \right) \quad (33)$$

instead of (32). Thus, in order to ensure that a relation like (31) still holds, we need to further require that $(\sigma_j^{ROM})^2$ is sufficiently small compared to σ_j^2 , $j = 1, \dots, s$;

- the correction shall result in a non normal distributed random variable (such as, e.g., when using REM3, where the correction is a multivariate log-normal random variable). In this case we cannot provide a closed-form expression for the K-L divergence. However, also in this case the key factors affecting the comparison between $D_{KL}(\pi^h || \tilde{\pi}^n)$ and $D_{KL}(\pi^h || \pi^n)$ are the same as in the previous case (as shown by the numerical results in the following section).

Let us now turn to evaluate how the corrections introduced through our REMs impact on the posterior PDFs. First of all, let us remark that, by taking the expectation of the K-L divergence between $\pi^h(\mathbf{s}^* | \boldsymbol{\mu})$ and $\pi^n(\mathbf{s}^* | \boldsymbol{\mu})$, and changing the order of integration, we obtain:

$$\mathbb{E}[D_{KL}(\pi^h || \pi^n)] = \int_{\mathcal{P}} D_{KL}(\pi^h || \pi^n) \pi_{prior}(\boldsymbol{\mu}) d\boldsymbol{\mu}. \quad (34)$$

Moreover, thanks to the positivity of the K-L divergence and relation (31), we get

$$\mathbb{E}[D_{KL}(\pi^h || \tilde{\pi}^n)] \leq \left(\max_{j=1, \dots, s} C_j^2 \right) \mathbb{E}[D_{KL}(\pi^h || \pi^n)]. \quad (35)$$

6.3 Posterior comparison for fixed n

We now want to compare the K-L divergences between the high-fidelity and the corrected/uncorrected posterior PDFs for small n . We can show the following

Proposition 4. *Under the same assumptions of Proposition 3,*

$$\mathbb{E}[D_{KL}(\pi_{post}^h || \tilde{\pi}_{post}^n)] \leq \mathbb{E}[D_{KL}(\pi_{post}^h || \pi_{post}^n)], \quad (36)$$

provided that the correction is made according to a deterministic REM.

Proof. Let us express the right-hand side of (36) as

$$\mathbb{E}[D_{KL}(\pi_{post}^h || \pi_{post}^n)] = \int_{\mathbb{R}^s} \left(\log \left(\frac{\eta_n(s)}{\eta_h(s)} \right) + \int_{\mathcal{P}} \frac{\pi^h(s|\boldsymbol{\mu})\pi_{prior}(\boldsymbol{\mu})}{\eta_h(s)} \log \left(\frac{\pi^h(s|\boldsymbol{\mu})}{\pi^n(s|\boldsymbol{\mu})} \right) d\boldsymbol{\mu} \right) \eta_h(s) ds. \quad (37)$$

In the same way, the left-hand side of (36) becomes

$$\mathbb{E}[D_{KL}(\pi_{post}^h || \tilde{\pi}_{post}^n)] = \int_{\mathbb{R}^s} \left(\log \left(\frac{\tilde{\eta}_n(s)}{\eta_h(s)} \right) + \int_{\mathcal{P}} \frac{\pi^h(s|\boldsymbol{\mu})\pi_{prior}(\boldsymbol{\mu})}{\eta_h(s)} \log \left(\frac{\pi^h(s|\boldsymbol{\mu})}{\tilde{\pi}^n(s|\boldsymbol{\mu})} \right) d\boldsymbol{\mu} \right) \eta_h(s) ds. \quad (38)$$

We proceed by analyzing separately the two terms of the right-hand side of (37). The second term coincides with (34), i.e.

$$\begin{aligned} & \int_{\mathbb{R}^s} \left(\int_{\mathcal{P}} \frac{\pi^h(s|\boldsymbol{\mu})\pi_{prior}(\boldsymbol{\mu})}{\eta_h(s)} \log \left(\frac{\pi^h(s|\boldsymbol{\mu})}{\pi^n(s|\boldsymbol{\mu})} \right) d\boldsymbol{\mu} \right) \eta_h(s) ds = \\ & = \int_{\mathcal{P}} \left(\int_{\mathbb{R}^s} \pi^h(s|\boldsymbol{\mu}) \log \left(\frac{\pi^h(s|\boldsymbol{\mu})}{\pi^n(s|\boldsymbol{\mu})} \right) ds \right) \pi_{prior}(\boldsymbol{\mu}) d\boldsymbol{\mu} = \mathbb{E}[D_{KL}(\pi^h || \pi^n)]. \end{aligned}$$

In the same way, the second term of the right-hand side of (38) is such that:

$$\int_{\mathbb{R}^s} \left(\int_{\mathcal{P}} \frac{\pi^h(s|\boldsymbol{\mu})\pi_{prior}(\boldsymbol{\mu})}{\eta_h(s)} \log \left(\frac{\pi^h(s|\boldsymbol{\mu})}{\tilde{\pi}^n(s|\boldsymbol{\mu})} \right) d\boldsymbol{\mu} \right) \eta_h(s) ds = \mathbb{E}[D_{KL}(\pi^h || \tilde{\pi}^n)].$$

On the other hand, by developing the first term of (37) with a Taylor expansion, we obtain:

$$\begin{aligned} \int_{\mathbb{R}^s} \log \left(\frac{\eta_n(s)}{\eta_h(s)} \right) \eta_h(s) ds &= \int_{\mathbb{R}^s} \left(\left(\frac{\eta_n(s)}{\eta_h(s)} - 1 \right) - \frac{1}{2} \left(\frac{\eta_n(s)}{\eta_h(s)} - 1 \right)^2 + \mathcal{O} \left(\frac{\eta_n(s)}{\eta_h(s)} - 1 \right)^3 \right) \eta_h(s) ds \\ &= \int_{\mathbb{R}^s} (\eta_n(s) - \eta_h(s)) ds - \int_{\mathbb{R}^s} \frac{1}{2} \left(\frac{\eta_n(s)^2}{\eta_h(s)} - 2\eta_n(s) + \eta_h(s) \right) ds + \int_{\mathbb{R}^s} \mathcal{O} \left(\frac{\eta_n(s)}{\eta_h(s)} - 1 \right)^3 \eta_h(s) ds. \end{aligned}$$

The first term of the last sum can be rewritten as

$$\int_{\mathbb{R}^s} (\eta_n(s) - \eta_h(s)) ds = \int_{\mathcal{P}} \left(\int_{\mathbb{R}^s} \pi^n(s|\boldsymbol{\mu}) ds \right) \pi_{prior}(\boldsymbol{\mu}) d\boldsymbol{\mu} - \int_{\mathcal{P}} \left(\int_{\mathbb{R}^s} \pi^h(s|\boldsymbol{\mu}) ds \right) \pi_{prior}(\boldsymbol{\mu}) d\boldsymbol{\mu}, \quad (39)$$

and it is vanishing, since

$$\int_{\mathcal{P}} \left(\int_{\mathbb{R}^s} \pi^h(s|\boldsymbol{\mu}) ds \right) \pi_{prior}(\boldsymbol{\mu}) d\boldsymbol{\mu} = \int_{\mathcal{P}} \left(\int_{\mathbb{R}^s} \pi^n(s|\boldsymbol{\mu}) ds \right) \pi_{prior}(\boldsymbol{\mu}) d\boldsymbol{\mu} = \int_{\mathcal{P}} \pi_{prior}(\boldsymbol{\mu}) d\boldsymbol{\mu} = 1.$$

In this way

$$\int_{\mathbb{R}^s} \log \left(\frac{\eta_n(s)}{\eta_h(s)} \right) \eta_h(s) ds = -\frac{1}{2} \int_{\mathbb{R}^s} \left(\frac{\eta_n(s)^2}{\eta_h(s)} - 1 \right) ds + \int_{\mathbb{R}^s} \mathcal{O} \left(\frac{\eta_n(s)}{\eta_h(s)} - 1 \right)^3 \eta_h(s) ds,$$

where we consider the integral of the remainder term of the Taylor expansion to be sufficient small when η_n/η_h is close to one, i.e. when the *likelihood* functions are very close to each other. For the same reason, the first term of the right-hand side of (38) behaves in the same way, so that

$$\begin{aligned} \mathbb{E}[D_{KL}(\pi_{post}^h || \tilde{\pi}_{post}^n)] &= -\frac{1}{2} \int_{\mathbb{R}^s} \left(\frac{\tilde{\eta}_n(s)^2}{\eta_h(s)} - 1 \right) ds + \mathbb{E}[D_{KL}(\pi^h || \tilde{\pi}^n)] + \int_{\mathbb{R}^s} \mathcal{O} \left(\frac{\tilde{\eta}_n(s)}{\eta_h(s)} - 1 \right)^3 \eta_h(s) ds \\ \mathbb{E}[D_{KL}(\pi_{post}^h || \pi_{post}^n)] &= -\frac{1}{2} \int_{\mathbb{R}^s} \left(\frac{\eta_n(s)^2}{\eta_h(s)} - 1 \right) ds + \mathbb{E}[D_{KL}(\pi^h || \pi^n)] + \int_{\mathbb{R}^s} \mathcal{O} \left(\frac{\eta_n(s)}{\eta_h(s)} - 1 \right)^3 \eta_h(s) ds. \end{aligned}$$

In conclusion, by using (35), inequality (36) follows under the following condition:

$$\begin{aligned} & \frac{1}{2} \int_{\mathbb{R}^s} \left(\frac{\eta_n(s)^2}{\eta_h(s)} - \frac{\tilde{\eta}_n(s)^2}{\eta_h(s)} \right) ds + \int_{\mathbb{R}^s} \mathcal{O} \left(\frac{\tilde{\eta}_n(s)}{\eta_h(s)} - 1 \right)^3 \eta_h(s) ds \\ & \leq \left(1 - \max_{j=1, \dots, s} C_j^2 \right) \mathbb{E}[D_{KL}(\pi^h || \pi^n)] + \int_{\mathbb{R}^s} \mathcal{O} \left(\frac{\eta_n(s)}{\eta_h(s)} - 1 \right)^3 \eta_h(s) ds, \end{aligned}$$

which can be seen as a robustness condition on the correction entailed by the REM. \square

7 Numerical results and discussion

We present two numerical examples illustrating the properties and the performance of the correction strategies proposed in Section 4. We recall that our final goal is to exploit fast and inexpensive *online* ROM queries by improving their accuracy through suitable REMs. For the cases at hand, uncertain parameters describe either the scalar conductivities over different subdomains or the continuous conductivity field over the whole domain. By measuring the average of the state solution over three boundary portions, identifiable parameters are reconstructed by marginalizing away the nuisance parameters. We provide a detailed analysis of the correction effects, by testing two different *prior* distributions.

7.1 Test case 1

We consider in $\Omega = (0, 1.5)^2$ the following diffusion problem:

$$\begin{cases} \nabla \cdot (k(\mathbf{x}, \boldsymbol{\mu}) \nabla u) = 0 & \text{in } \Omega \\ k(\mathbf{x}, \boldsymbol{\mu}) \nabla u \cdot \mathbf{n} = 0 & \text{on } \Gamma_w \\ k(\mathbf{x}, \boldsymbol{\mu}) \nabla u \cdot \mathbf{n} = 1 & \text{on } \Gamma_b \\ u = 0 & \text{on } \Gamma_t, \end{cases} \quad (40)$$

where $\partial\Omega = \Gamma_w \cup \Gamma_b \cup \Gamma_t$ (see Fig. 1, left). Here $k(\mathbf{x}, \boldsymbol{\mu})$ is a parametrized diffusion coefficient:

$$k(\mathbf{x}, \boldsymbol{\mu}) = 0.1 \mathbb{I}_{\Omega_0}(\mathbf{x}) + \sum_{i=1}^3 \mu_i \mathbb{I}_{\Omega_i}(\mathbf{x}),$$

where \mathbb{I}_{Ω_i} is the characteristic function of the subdomains : $\Omega_1 = (0, 0.5)^2 \cup (1, 1.5)^2$, $\Omega_2 = (0, 0.5) \times (1, 1.5) \cup (1, 1.5) \times (0, 0.5)$, $\Omega_3 = (0.5, 1)^2$ and $\Omega_0 = \Omega \setminus \bigcup_{i=1}^3 \Omega_i$. Finally, the outputs are given by

$$s^j(\boldsymbol{\mu}) = \int_{\Gamma_j} u(\boldsymbol{\mu}) d\Gamma, \quad j = 1, 2, 3.$$

Our objective is to identify $\gamma = \mu_3$ by observing the outputs $s^j(\boldsymbol{\mu})$, $j = 1, 2, 3$, in presence of two nuisance parameters $\boldsymbol{\zeta} = (\mu_1, \mu_2)$. We suppose that the target value \mathbf{s}^* corresponds to the full order output vector evaluated for $\gamma^* = 2$ and a random value of $\boldsymbol{\zeta}$.

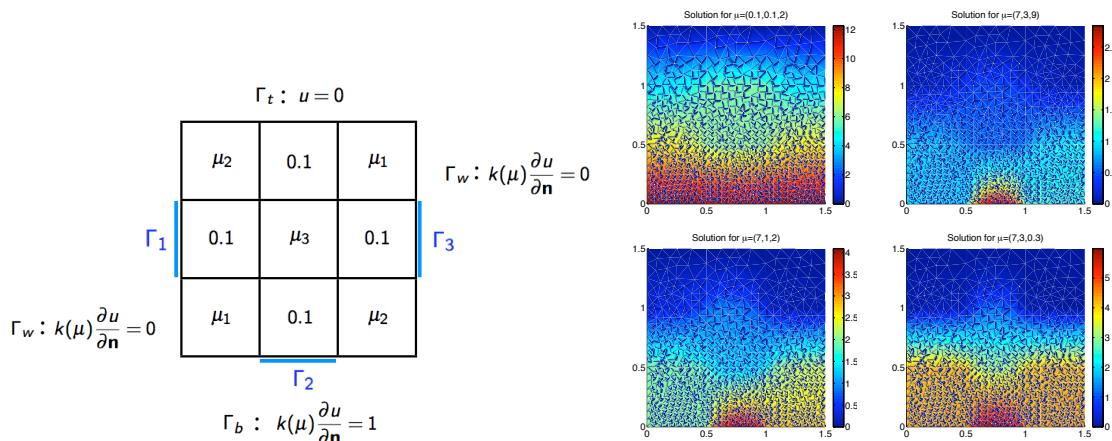


Figure 1: Test case 1: domain, boundary conditions (left) and different sample solutions of 40 (right).

The forward problem (40) is first discretized using the FE approach with P1 elements, which generates a total of $\mathcal{N}_h = 1,056$ degrees of freedom. In view of the application of the MCMC algorithm, we adopt the RB method: we stop the greedy algorithm after selecting $n = 10$ basis functions for the forward problem and for each dual problem related to one of the three outputs, in view of the analysis of the corrections effects.

We intentionally select few basis functions (satisfying a tolerance $\epsilon_{RB}^{tol} = 5 \cdot 10^{-2}$) in order to assess the capability of our REMs in correcting the outcome of a possible inaccurate ROM. Note that for more complex (e.g. non-affine and/or non-linear) problems a potentially very large number of basis functions is required to guarantee a sufficient accuracy, with a consequent loss of efficiency. As a matter of fact, we reach in our case a considerable speedup ($n/\mathcal{N}_h \simeq 1/100$). Nevertheless, output evaluations are affected by ROM errors, which have to be taken into account by the correction methods. To this aim, we construct a calibration set of $N_{cal} = 100$ points in the parameter space from a Gauss-Patterson sparse grid⁶, from which we calculate the full-order FE as well as the RB solutions and the relative outputs. In this way, we obtain a sample of outputs ROM errors, upon which we calibrate the proposed REMs. This operation can be performed in parallel and does not impact significantly on the offline complexity.

Before analyzing the quality of the corrections, we provide few details related to REMs construction. By a direct inspection of the errors sample generated over the calibration set, we remark that their distribution is far from being Gaussian (Fig. 2).

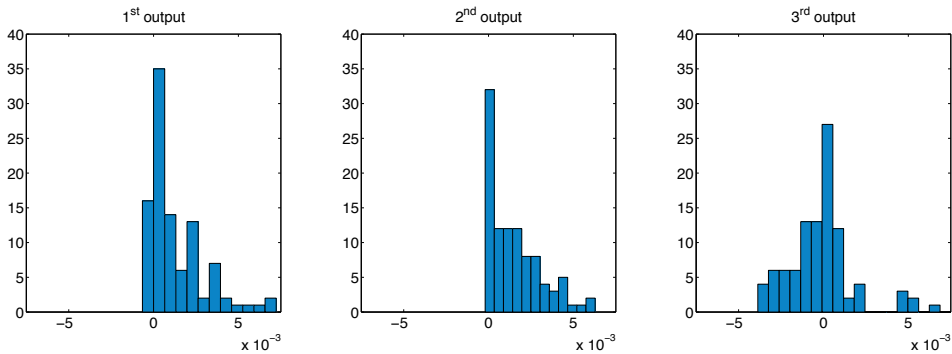


Figure 2: Histogram of the ROM errors for each output $s^j(\boldsymbol{\mu})$, $j = 1, 2, 3$.

The Shapiro-Wilk test rejects for all the outputs the null hypothesis that the errors come from a normal distribution ($p\text{-value} < 10^{-5}$ in all cases). Moreover, errors are not equally distributed over the parameter space: for this reason $\boldsymbol{\mu}$ -dependent approaches (like REM-2 and REM-3) should better capture the error variability. Concerning REM-2, we point out that the approach relying on error bound effectivities is preferable to the one based on ROM errors if we aim at minimizing the maximum norm of the interpolation error (see Fig. 3).

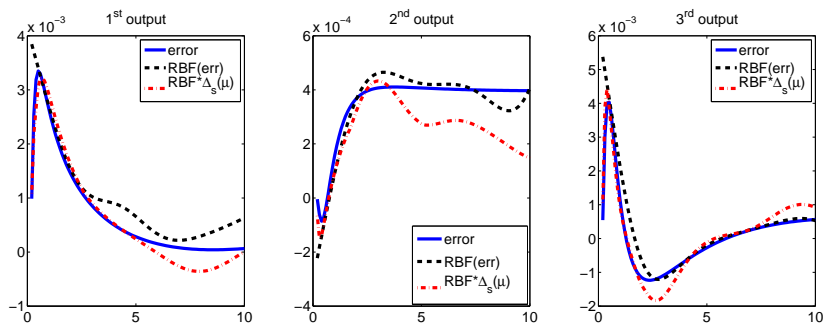


Figure 3: Comparison between the RBF interpolation of the inverse effectivities and of the ROM errors for each output $s^j(\boldsymbol{\mu})$, $j = 1, 2, 3$, on varying μ_3 ($\mu_1 = 7$, $\mu_2 = 3$).

Furthermore, for REM-3, a linear regression model on the log-variable is fitted for each output and by distinguishing the errors sign. (see Fig. 4). It is not surprising that models providing a better fitting are those built on larger datasets, even if the Bernoulli sign trick proposed in Section 4.3 contributes to filter out those models built on smaller samples.

⁶However, in the test cases very similar results in terms of calibration performances can be obtained by relying on a random sampling of the parameter space, due to the small parametric dimension.

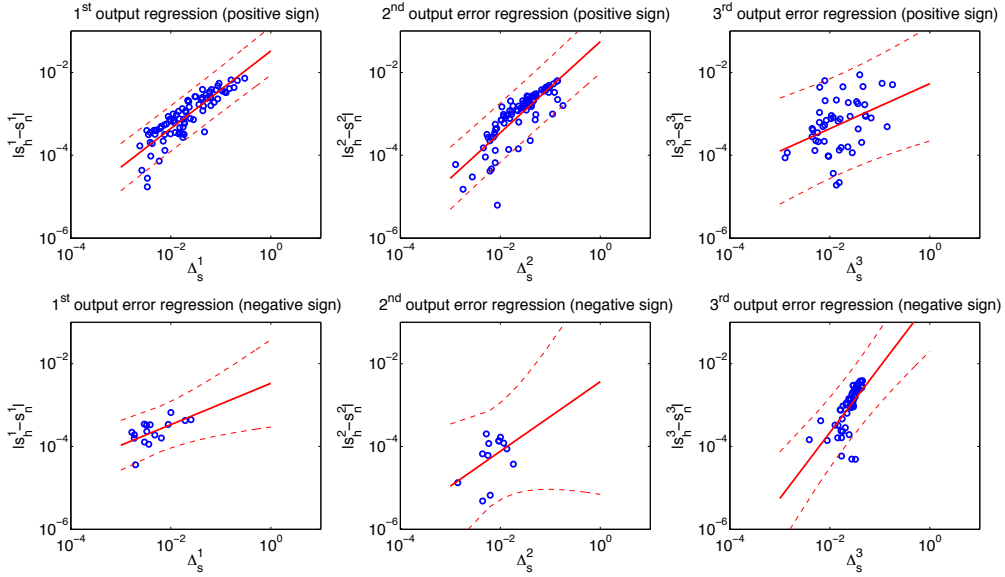


Figure 4: Linear regression (in the log / log space) of the ROM errors against error bounds and 95% confidence intervals. Prediction confidence bands (around the regression line) for the predicted value are obtained by considering the standard error and the 95% quantiles of the $t(N_{cal}^+ - 2)$ (resp. $t(N_{cal}^- - 2)$) distribution, where N_{cal}^+ (resp. N_{cal}^-) is the sample size of positive (resp. negative) errors.

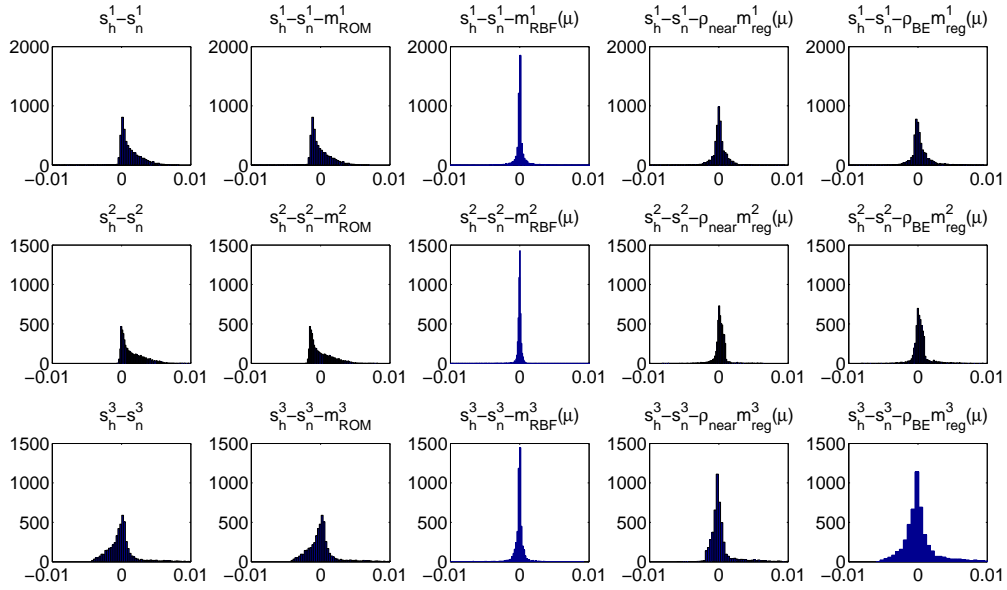


Figure 5: Comparison between the REM reconstruction of the errors for s^1 , s^2 and s^3 (from top to bottom).

A primary test for assessing the quality of our REMs has been made by considering a random sample of 5000 points in \mathcal{P} and computing the frequencies of ROM errors and the corresponding quantities corrected according to the three REMs (see Fig. 5). As expected, REM-1 results in a simple shift of the errors distribution. On the other hand, the distributions of the errors in presence of μ -dependent approaches (REM-2 and REM-3) show a more symmetric shape, with mean closer to zero and smaller variance than in the ROM errors distributions. Sample means and standard deviations are reported in Table 1. Hence, the μ -dependent approaches allow to reduce the ROM error by at least one order of magnitude. REM-2 performs very well in this case, although it can suffer from the curse of dimensionality.

	$j = 1$	$j = 2$	$j = 3$
No REM	$1.2 \cdot 10^{-3}$ ($1.5 \cdot 10^{-3}$)	$1.5 \cdot 10^{-3}$ ($1.6 \cdot 10^{-3}$)	$2.6 \cdot 10^{-3}$ ($2.2 \cdot 10^{-3}$)
REM-1	$-5.6 \cdot 10^{-5}$ ($1.5 \cdot 10^{-3}$)	$5.3 \cdot 10^{-5}$ ($1.6 \cdot 10^{-3}$)	$9.2 \cdot 10^{-5}$ ($2.2 \cdot 10^{-3}$)
REM-2	$4 \cdot 10^{-5}$ ($1.3 \cdot 10^{-3}$)	$-1.6 \cdot 10^{-4}$ ($1.4 \cdot 10^{-3}$)	$-2.5 \cdot 10^{-4}$ ($2.1 \cdot 10^{-3}$)
REM-3 near	$7.4 \cdot 10^{-5}$ ($1 \cdot 10^{-3}$)	$1.9 \cdot 10^{-4}$ ($8.7 \cdot 10^{-4}$)	$2.6 \cdot 10^{-4}$ ($1.9 \cdot 10^{-3}$)
REM-3 Be	$2.2 \cdot 10^{-4}$ ($1.3 \cdot 10^{-3}$)	$3.5 \cdot 10^{-4}$ ($1.1 \cdot 10^{-3}$)	$3.4 \cdot 10^{-4}$ ($3 \cdot 10^{-3}$)
	$p = 0.84$	$p = 0.87$	$p = 0.49$

Table 1: Sample means (and standard deviations) for the output of the errors obtained with each REM.

Then, we have applied the MCMC algorithm to reconstruct the unknown parameters values, by sampling the reduced posterior distribution (corrected by the three different REMs). For REM-1, since the distribution of the calibration ROM errors is far from being Gaussian, we have fitted log-normal distribution (see Fig. 6), consistently with the ability of identifying the sign through appropriate criteria introduced in Section 4.3. However, also with this choice we do not get a significant improvement on the accuracy of the corrected posterior (see Fig. 6, right). On the other hand, the good results in terms of error correction provided by REM-2 and REM-3 enhance also the evaluation of corrected reduced posteriors (see Fig. 7, left). Moreover, by considering also statistical correction (Fig. 7, right), we get maximum a-posteriori estimates close to the high-fidelity one, even if this procedure generates heavy-tailed *posterior* distributions and consequently less tight a posteriori prediction intervals.

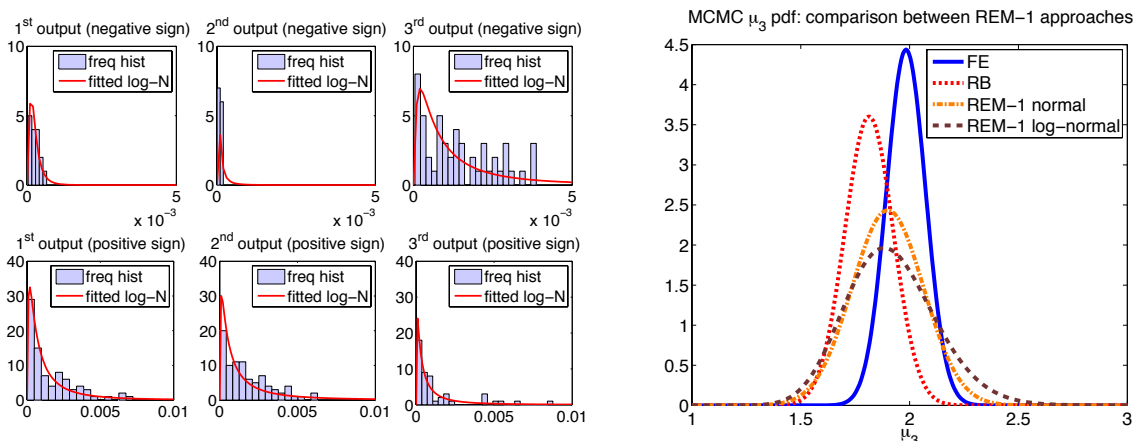


Figure 6: Distribution of the output errors divided by the sign (left) and the corrected reduced posterior obtained by REM1 correction (right): π_{post}^h in blue, π_{post}^n in red and $\tilde{\pi}_{post}^n$ in orange based on Gaussian distribution and in brown based on log-normal distribution. Here a uniform *prior* distribution is considered.

So far we have considered a uniform prior distribution. If we turn to a Gaussian *prior*, numerical results still confirm a good behavior of REM-2 and REM-3, and a worse performance of REM-1. In this case, we have tested a situation of wrong a priori input with low confidence on it, i.e. $\mu_{p,3} = 3$ and variance $\sigma_i^2 \delta_{ii} = 1$, $1 \leq i \leq s$. As before, we are able to get a good reconstruction of the high-fidelity posterior distribution for REM-2 and REM-3 (see Fig. 8). Finally, as a validation of the theoretical results presented in Section 6, we report in Table 2 the maximum a-posteriori (MAP) estimates, the 95% credibility intervals and the KL-divergences for the three REMs and both prior distributions. We are able to verify the relation between REMs corrections and K-L divergences of Proposition 4. However, this relation does not hold in presence of a significant variance associated with the correction (in this case the K-L divergence increases).

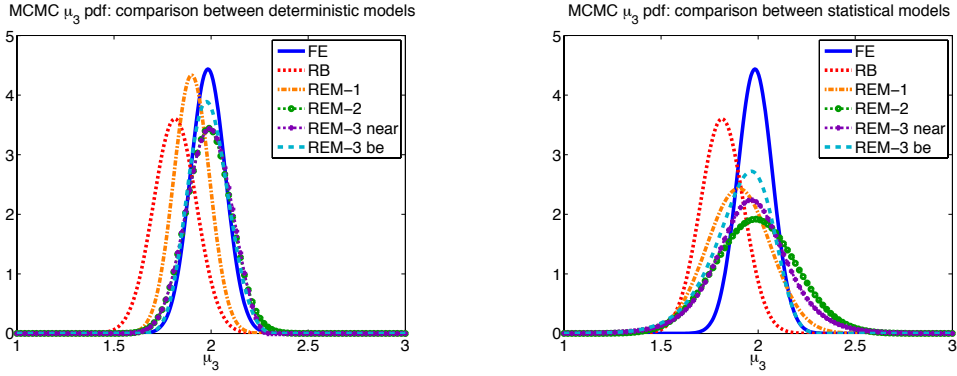


Figure 7: Posterior distributions obtained with deterministic (left) and statistical (right) corrections. π_{post}^h is represented in blue, π_{post}^n in red, $\tilde{\pi}_{post}^n$ in orange for REM-1, in green for REM-2 and in purple and light blue for REM-3 on varying the sign corrections. Here a uniform prior distribution is considered.

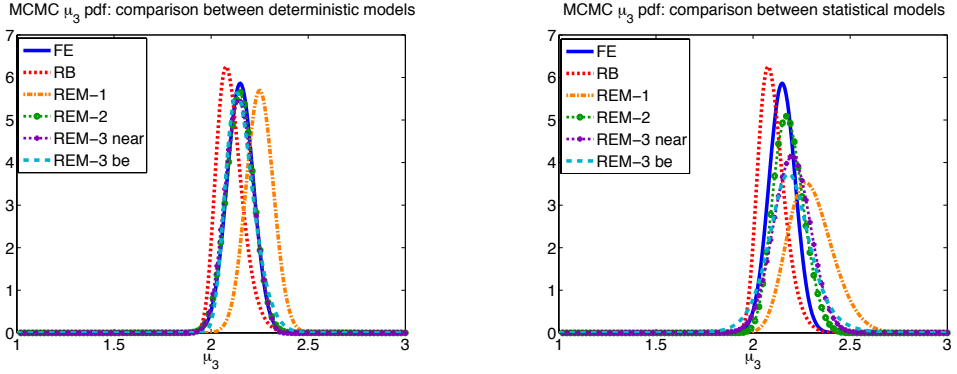


Figure 8: Posterior distributions obtained with deterministic (left) and statistical (right) REMs in the case of Gaussian *prior* distribution.

	uniform prior			Gaussian prior		
	μ_{MAP}	CI 95%	KL-dist	μ_{MAP}	CI 95%	KL-dist
FE	1.9837	(1.8075, 2.1598)		2.1498	(2.0166, 2.2830)	
RB	1.8139	(1.5968, 2.0311)	1.2152	2.0776	(1.9879, 2.2499)	0.2936
REM-1	1.8997	(1.5783, 2.2213)	0.3829	2.2726	(2.0986, 2.5446)	1.0856
REM-2	1.9881	(1.7608, 2.2150)	0.0555	2.1493	(2.0110, 2.2876)	0.0014
REM-3 (near)	1.9917	(1.7623, 2.1898)	0.0516	2.1420	(2.0102, 2.2818)	0.0213
REM-3 (near+var)	1.9719	(1.4932, 2.4501)	0.3423	2.2121	(2.0224, 2.4017)	0.3064
REM-3 (BE)	1.9754	(1.7988, 2.1858)	0.0131	2.1331	(2.0329, 2.3228)	0.0124
REM-3 (BE+var)	1.9645	(1.5546, 2.3723)	0.2474	2.1830	(1.9553, 2.4464)	0.2538

Table 2: MAP estimates, 95% empirical prediction intervals and K-L divergences from the posterior FE distribution.

7.2 Test case 2

We modify problem (40) by considering a parametric field description of the diffusion coefficient $k(\mathbf{x})$: all the possible configurations of the field are generated from a standard multivariate Gaussian of dimension \mathcal{N}_h (we deal in this case with a \mathbb{P}^1 FE discretization). To reduce this complexity, we assume the field as generated by a multivariate Gaussian distribution with covariance matrix

$$C_{ij} = a \exp\left(-\frac{\|x_i - x_j\|}{2b^2}\right) + c\delta_{ij} \quad \forall i, j = 1, \dots, \mathcal{N}_h,$$

$a, b, c > 0$ and $\{x_i\}_{i=1}^{\mathcal{N}_h}$ are the nodes of the computational mesh.

A further simplification is obtained by considering a Karhunen-Loève expansion of the random field, which identifies the d most relevant (independent) eigenmodes $\xi_1, \xi_2, \dots, \xi_d$ of the covariance operator C corresponding to the largest eigenvalues $\lambda_1(C) \geq \lambda_2(C) \geq \dots \geq \lambda_d(C)$. The same result can be achieved by computing the POD of a set of random fields generated accordingly to the proposed distribution. The field description then reduces to

$$k(\mathbf{x}, \boldsymbol{\mu}) = 3.5 + \sum_{i=1}^d \mu_i \sqrt{\lambda_i} \xi_i \quad (41)$$

where μ_i , $1 \leq i \leq d$, will play the role of identifiable parameters (each one a priori distributed as a standard Gaussian). In this way the sampling is done in a d -dimensional space, with $d \ll \mathcal{N}_h = 1,572$. By taking for the covariance matrix $a = 1$, $b = 0.6$ and $c = 10^{-8}$, we explain about the 90% of the variance by taking $d = 4$ modes (see Fig. 9, top). We also consider the presence of four nuisance parameters (see Fig. 9, bottom), which describe the presence of localized distortions z_i of the parametric field given by:

$$\sum_{i=1}^4 \boldsymbol{\mu}_{4+i} z_i(\mathbf{x}) = \sum_{i=1}^4 \boldsymbol{\mu}_{4+i} \exp\left(-\frac{(x-x_i)^2 + (y-y_i)^2}{0.025}\right), \quad (42)$$

where $\mathbf{x} = [0.25, 0.25, 1.25, 1.25]$ and $\mathbf{y} = [0.25, 1.25, 1.25, 0.25]$.

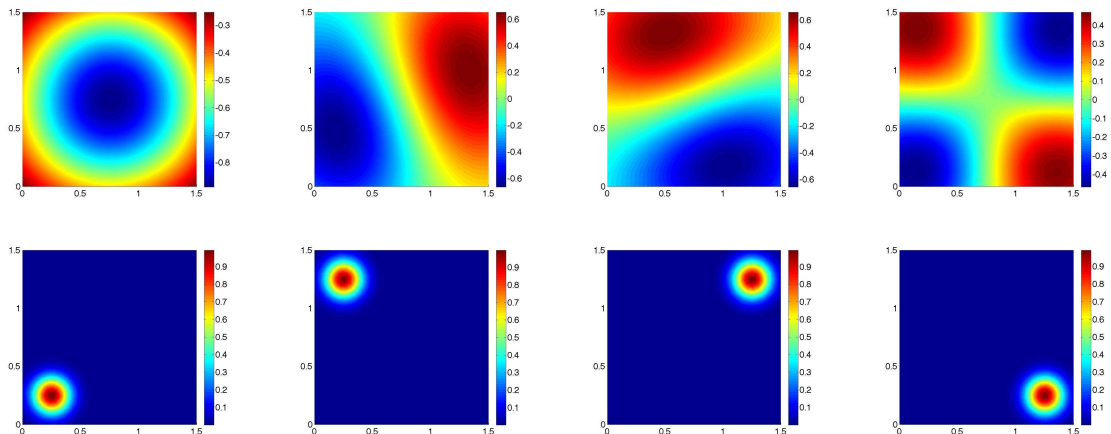


Figure 9: Top: first most relevant modes u_i , $i = 1, \dots, 4$, of the Karhunen-Loève expansion. Bottom: Four nuisance modes z_i , $i = 1, \dots, 4$.

In this case, the inverse problem consists in identifying the *posterior* distributions of μ_i , $1 \leq i \leq 4$, by observing the outputs $s^j(\boldsymbol{\mu})$, $j = 1, 2, 3$, in presence of the four nuisance parameters μ_i , $5 \leq i \leq 8$. We consider as a target values $\mathbf{s}^* = \mathbf{s}(\boldsymbol{\mu}^*)$, where $\boldsymbol{\mu}^* = [\boldsymbol{\gamma}^*, \boldsymbol{\zeta}^*]$ and $\boldsymbol{\gamma}^* = (-1, 0.5, -0.6, -0.8)$ whereas $\boldsymbol{\zeta}^*$ is chosen randomly. We build a RB approximation of the state and the dual problems associated to each of the three outputs; $n = 20$ basis functions are selected for each of this four problems. This yields a reduction error on the outputs, that has been treated with the proposed REMs, built on a calibration set of $N_{cal} = 100$ values.

A primary test to assess the quality of the different corrections has been performed by considering a random set of 5000 points over \mathcal{P} , and evaluating the frequencies of the errors on the three outputs together with the corrections provided by the three REMs (see Fig. 10 and Table 3). REM-1 (with a Gaussian distribution for the approximation error model) is effective only for the second output $s^2(\boldsymbol{\mu})$ but provides a worse correction for $s^1(\boldsymbol{\mu})$ and $s^3(\boldsymbol{\mu})$. On the other hand, the distribution of the errors corrected with REM-2 and REM-3 approaches are very similar, yielding a more symmetric distribution, which shows in both cases a mean closer to zero than the ROM errors one.

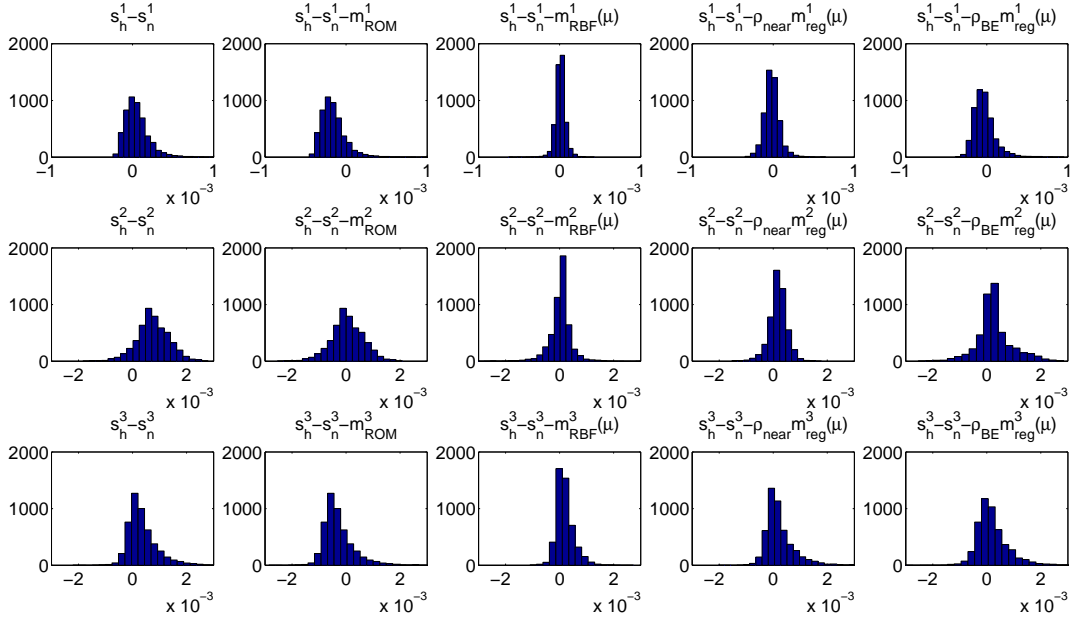


Figure 10: Comparison between the REM reconstruction of the errors for s^1 , s^2 , s^3 (from top to bottom).

	$i = 1$	$i = 2$	$i = 3$
No REM	$5.5 \cdot 10^{-5}$ ($1.5 \cdot 10^{-4}$)	$7.5 \cdot 10^{-4}$ ($6 \cdot 10^{-4}$)	$3.8 \cdot 10^{-4}$ ($6.2 \cdot 10^{-4}$)
REM-1	$-1.5 \cdot 10^{-4}$ ($1.5 \cdot 10^{-4}$)	$4.3 \cdot 10^{-5}$ ($6 \cdot 10^{-4}$)	$-2.7 \cdot 10^{-4}$ ($6.2 \cdot 10^{-4}$)
REM-2	$1 \cdot 10^{-5}$ ($6.3 \cdot 10^{-5}$)	$3.9 \cdot 10^{-5}$ ($4 \cdot 10^{-4}$)	$1.9 \cdot 10^{-5}$ ($3.3 \cdot 10^{-4}$)
REM-3 near	$-1.6 \cdot 10^{-5}$ ($9.4 \cdot 10^{-5}$)	$1.8 \cdot 10^{-4}$ ($3.3 \cdot 10^{-4}$)	$2.6 \cdot 10^{-4}$ ($5.7 \cdot 10^{-4}$)
REM-3 Be	$-2.9 \cdot 10^{-5}$ ($1.3 \cdot 10^{-4}$)	$2.7 \cdot 10^{-4}$ ($6 \cdot 10^{-4}$)	$2.1 \cdot 10^{-4}$ ($6.2 \cdot 10^{-4}$)
	$p = 0.61$	$p = 0.82$	$p = 0.80$

Table 3: Sample means (and standard deviations) for the output of the errors obtained with each REM.

We then apply the MCMC procedure and we evaluate the effect of the proposed REMs on the posterior distributions. The previous analysis of error corrections reflects also on the posterior distribution: as shown in Fig. 11, REM-2 is more effective than REM-1. We report the maximum a-posteriori (MAP) estimates for each identifiable parameters and the KL-divergences for each REM in Table 4, and the 95% prediction intervals for the MAP estimates in Table 5; these results confirm the efficacy of the deterministic correction provided by REM-2 and REM-3. Moreover, for the identification of μ_3 and μ_4 , the presence of the statistical correction does not lead to an increasing of K-L divergence values.

REM-3 is the most effective model in the correction of the posterior distribution (see Figs. 12-13); not only, results are not significantly affected by the additional variance, to be included when we consider the statistical correction.

Finally, we evaluate the diffusivity field (41) for the different MAP estimates, recovered a posteriori by considering different REMs (see Fig. 14). In order to quantify the difference between the *target* field and the fields obtained through the inversion procedure, we compute the $L^2(\Omega)$ -norm of their difference (see Table 6). As expected, the most distant field is the one obtained with the RB method without corrections, while the presence of the REMs improves substantially the reconstruction of the field. In conclusion, the best performance in term of parameters identification is provided by REM-3 based on both the sign correction strategies.

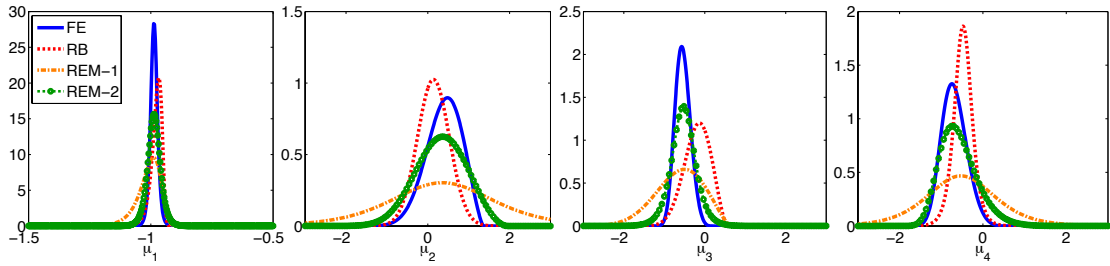


Figure 11: Marginal posterior distribution for the four parameters of interest: the posterior full-order PDF π_{post}^h is in blue, π_{post}^n in red and $\tilde{\pi}_{post}^n$ in orange with REM1 correction and in green with REM2.

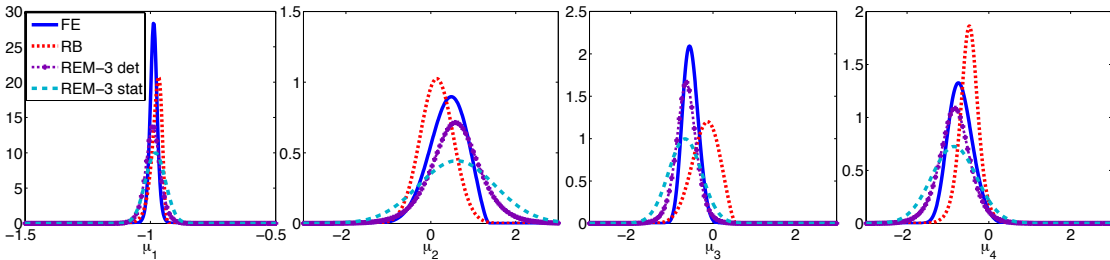


Figure 12: Marginal posterior distribution for the four parameters of interest with REM3 corrections and sign model with nearest neighbor strategy. The posterior full-order PDF π_{post}^h is in blue, π_{post}^n in red and $\tilde{\pi}_{post}^n$ in purple and in light blue respectively for the deterministic and the statistical correction.

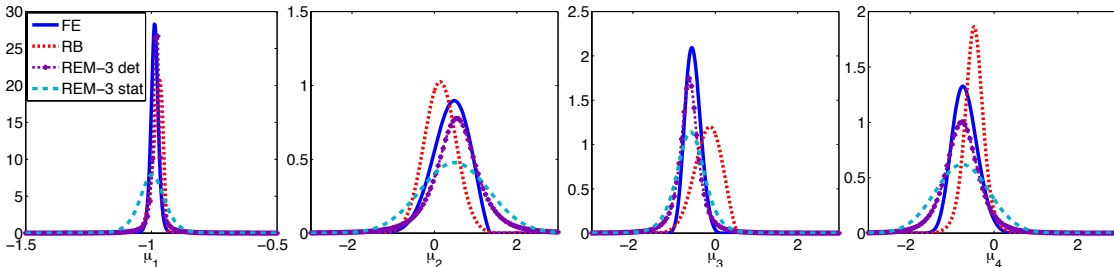


Figure 13: Marginal posterior distribution for the four parameters of interest with REM3 corrections and sign model as a Bernoulli process.

7.3 Computational performance

Thanks to our RB method, we improved the computational performance of the MCMC algorithm by decreasing the cost of each online evaluation. In both the test cases we considered, we observe that the impact of the REM calibration on the *offline* phase is negligible (less than 10%).

Moreover, each *online* query (even in presence of the various REMs) takes about 10^{-4} s in both test cases, and the *offline* cost is amortized very fast, due to the huge number – $\mathcal{O}(10^6)$ – of iterations required by the MCMC algorithm.

This latter takes less than 1h, compared to more than 6h when relying on the high-fidelity model. The proposed REMs enable to recover very accurate *online* evaluations of the outputs of the forward problem by properly correcting the RB outcome during the *online* stage.

	μ_1^{MAP}	D_{KL}	μ_2^{MAP}	D_{KL}	μ_3^{MAP}	D_{KL}	μ_4^{MAP}	D_{KL}
FE	-0.987		0.482		-0.571		-0.743	
RB	-0.967	0.327	0.139	0.241	-0.132	0.849	-0.476	0.439
REM-1	-0.988	0.575	0.356	0.713	-0.504	0.722	-0.528	0.657
REM-2	-0.986	0.205	0.3047	0.132	-0.526	0.177	-0.732	0.121
REM-3 (near)	-0.997	0.288	0.584	0.166	-0.657	0.179	-0.831	0.142
REM-3 (near+var)	-0.953	0.530	0.614	0.409	-0.687	0.432	-0.852	0.309
REM-3 (BE)	-0.980	0.221	0.546	0.154	-0.632	0.195	-0.770	0.146
REM-3 (BE+var)	-0.997	0.753	0.488	0.330	-0.601	0.313	-0.760	0.390

Table 4: MAP estimates for the identifiable parameters and KL-divergences from the FE posterior distributions.

	μ_1^{MAP} CI	μ_2^{MAP} CI	μ_3^{MAP} CI	μ_4^{MAP} CI
FE	(-1.02, -0.95)	(-0.52, 1.12)	(-0.89, -0.16)	(-1.23, -0.07)
RB	(-1.032, -0.944)	(-0.624, 0.902)	(-0.864, 0.361)	(-0.967, 0.015)
REM-1	(-1.130, -0.938)	(-2.675, 3.000)	(-1.902, 0.335)	(-2.488, 1.433)
REM-2	(-1.045, -0.928)	(-1.392, 1.707)	(-1.182, 0.129)	(-1.321, 0.458)
REM-3 (near)	(-1.070, -0.924)	(-0.906, 2.135)	(-1.354, -0.021)	-1.8094, 0.103
REM-3 (near+var)	(-1.017, -0.890)	(-1.203, 2.371)	(-1.433, 0.119)	(-2.059, 0.396)
REM-3 (BE)	(-1.067, -0.892)	(-0.930, 2.021)	(-1.395, 0.133)	(-1.806, 0.266)
REM-3 (BE+var)	(-1.113, -0.881)	(-1.151, 2.127)	(-1.403, 0.200)	(-2.020, 0.502)

Table 5: 95% empirical prediction intervals for each MAP estimator for different REMs.

	RB	REM-1	REM-2	REM-3(near)	REM-3(Be)
$\ \cdot\ _{L^2(\Omega)}$	0.328	0.146	0.099	0.060	0.045

Table 6: $L^2(\Omega)$ -norm of the distance between the reconstructed field for different REMs and the target one.

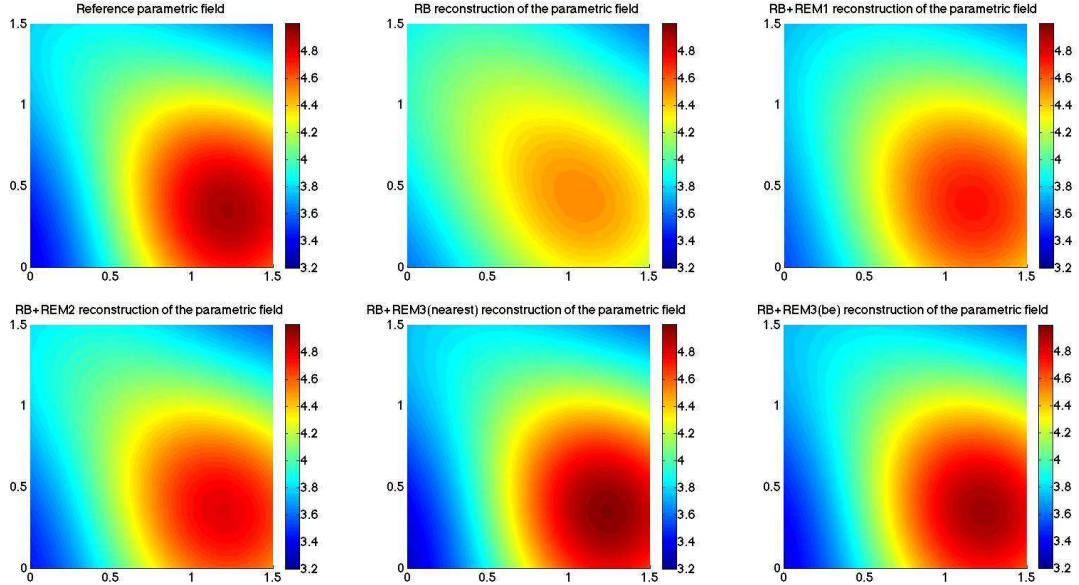


Figure 14: Diffusivity field reconstructed by means of the different REMs (parameters values identified with maximum a posteriori estimators).

Approximation data	test 1	test 2	Performances	test 1	test 2
Number of FE dofs \mathcal{N}_h	1,056	1,572	MCMC iterations	$5 \cdot 10^5$	10^6
Number of RB dofs n	10	20	ROM solution	$2 \cdot 10^{-4}$ s	$3 \cdot 10^{-4}$ s
Dofs reduction	101:1	79:1	ROM error bound	$4 \cdot 10^{-4}$ s	$8.2 \cdot 10^{-4}$ s
Number of parameters	3	8	REM-1	≈ 0 s	≈ 0 s
FE solution	$4 \cdot 10^{-2}$ s	$1.3 \cdot 10^{-1}$ s	REM-2	$7.5 \cdot 10^{-4}$ s	$1.32 \cdot 10^{-3}$ s
Offline: basis computation	134 s	776 s	REM-3 (near)	$7 \cdot 10^{-4}$ s	$1.12 \cdot 10^{-3}$ s
Offline: REM calibration	13 s	24 s	REM-3 (Be)	$4 \cdot 10^{-4}$ s	$8.2 \cdot 10^{-4}$ s

Table 7: Computational performances of the proposed framework for both test cases

References

- [1] S. R. ARRIDGE, J. P. KAIPIO, V. KOLEHMAINEN, M. SCHWEIGER, E. SOMERSALO, T. TARVAINEN, AND V. VAUHKONEN, Approximation errors and model reduction with an application in optical diffusion tomography, *Inverse Problems*, 22(1):175–195, 2006.
- [2] I. BABUŠKA, F. NOBILE, AND R. TEMPONE, A stochastic collocation method for elliptic partial differential equations with random input data, *SIAM Review*, 52(2):317–355, 2010.
- [3] H. T. BANKS, M. L. JOYNER, B. WINCHESKI, AND W. P. WINFREE, Nondestructive evaluation using a reduced-order computational methodology, *Inverse Problems*, 16(4):929, 2000.
- [4] L. BIEGLER, G. BIROS, O. GHATTAS, M. HEINKENSCHLOSS, D. KEYES, B. MALLICK, Y. MARZOUK, B. VAN BLOEMEN WAANDERS, AND K. WILLCOX (Eds.), *Large-Scale Inverse Problems and Quantification of Uncertainty*, pages 123–149. John Wiley & Sons, Ltd, 2010.
- [5] A. BIROLLEAU, G. POËTTE, AND D. LUCOR, Adaptive Bayesian inference for discontinuous inverse problems, application to hyperbolic conservation laws, *Commun. Comput. Phys.*, 16(1):1–34, 2014.
- [6] M. D. BUHMANN, Radial basis functions, *Acta Numerica*, 9: 1–38, 2000.
- [7] T. BUI-THANH, AND O. GHATTAS, An analysis of infinite dimensional Bayesian inverse shape acoustic scattering and its numerical approximation, *SIAM J. Uncert. Quant.*, submitted, 2012.
- [8] M. CHEVREUIL, AND A. NOUY, Model order reduction based on proper generalized decomposition for the propagation of uncertainties in structural dynamics, *Int. J. Numer. Meth. Engng.*, 89(2):241–268, 2012.
- [9] T. CUI, Y. M. MARZOUK, AND K. WILLCOX, Data-Driven Model Reduction for the Bayesian Solution of Inverse Problems, *arXiv:1403.4290 e-prints*, 2014.
- [10] M. DROHMANN, AND K. C. CARLBERG, The ROMES method for statistical modeling of reduced-order-model error, *arxiv:1405.5170 e-prints*, 2014.
- [11] A. F. EMERY, AND A. JOHNSON, Model order reduction based on proper generalized decomposition for the propagation of uncertainties in structural dynamics, *Int. J. Numer. Meth. Engng.*, 89(2):241–268, 2012.
- [12] D. GALBALLY, K. FIDKOWSKI, K. WILLCOX, AND O. GHATTAS, Nonlinear model reduction for uncertainty quantification in large-scale inverse problems, *Int. J. Numer. Methods Engng*, 81(12):1581–1608, 2010.
- [13] R. G. GHANEM, AND P. D. SPANOS, Stochastic finite elements: a spectral approach, *Springer*, 1991.
- [14] W. R. GILKS, S. RICHARDSON, AND D. J. SPIEGELHALTER, Markov Chain Monte Carlo in practice, *CRC press*, volume 2., 1995.
- [15] J. C. HELTON, J. D. JOHNSON, C. J. SALLABERRY, AND C. B. STORLIE, Survey of sampling-based methods for uncertainty and sensitivity analysis, *Reliab. Eng. Syst. Saf.*, 91(10):1175–1209, 2006.
- [16] J. JAKEMAN, M. ELDRED, AND D. XIU, Numerical approach for quantification of epistemic uncertainty, *J. Comput. Phys.*, 229:4648–4663, 2010.
- [17] J. KAIPIO, AND E. SOMERSALO, Statistical and computational inverse problems, *Springer Science+Business Media, Inc.*, 2005.
- [18] T. LASSILA, A. MANZONI, A. QUARTERONI, AND G. ROZZA, Generalized reduced basis methods and n -width estimates for the approximation of the solution manifold of parametric PDEs. *Bollettino UMI, Serie IX, Vol. VI (1):113–135*, 2013.
- [19] T. LASSILA, A. MANZONI, A. QUARTERONI, AND G. ROZZA, A reduced computational and geometrical framework for inverse problems in haemodynamics, *Int. J. Numer. Methods Biomed. Engng.*, 29(7):741–776, 2013.

- [20] T. LASSILA, A. MANZONI, A. QUARTERONI, AND G. ROZZA, Model order reduction in fluid dynamics: challenges and perspectives. In A. Quarteroni and G. Rozza, editors, *Reduced Order Methods for Modeling and Computational Reduction*, volume 9, pages 235–274. Springer, MS&A Series, 2014.
- [21] Y. LI, AND Y. M. MARZOUK Adaptive construction of surrogates for the Bayesian solution of inverse problems, *arXiv:1309.5524 e-prints*, 2013.
- [22] J. S. LIU Monte Carlo strategies in Scientific Computing, Springer, New York, 2001.
- [23] C. LIEBERMAN, K. WILLCOX, AND O. GHATTAS, Parameter and state model reduction for large-scale statistical inverse problems, *SIAM J. Sci. Comput.*, 32(5):2523–2542, 2010.
- [24] A. LIPPONEN, A. SEPPÄNEN ,AND J. P. KAIPIO, Reduced-order model for electrical impedance tomography based on proper orthogonal decomposition, *arXiv:1207.0914 e-prints*, 2012.
- [25] A. MANZONI, AND F. NEGRI, Rigorous and heuristic strategies for the approximation of stability factors in nonlinear parametrized PDEs, *Technical report MATHICSE 8.2014, submitted*, 2014.
- [26] J. MARTIN, L. C. WILCOX, C. BURSTEDDE, AND O. GHATTAS, A stochastic Newton MCMC method for large-scale statistical inverse problems with application to seismic inversion, *SIAM J. Sci. Comput.*, 34(3):A1460–A1487, 2012.
- [27] Y. M. MARZOUK, AND H. N. NAJM, Dimensionality reduction and polynomial chaos acceleration of Bayesian inference in inverse problems, *J. Comput. Phys.*, 228:1862–1902, 2009.
- [28] Y. M. MARZOUK, AND D. XIU, A Stochastic Collocation Approach to Bayesian Inference in Inverse Problems, *Commun. Comput. Phys.*, 6(4):826–847, 2009.
- [29] L. W. T. NG, AND M. S. ELDRED, Multifidelity Uncertainty Quantification Using Nonintrusive Polynomial Chaos and Stochastic Collocation, *paper AIAA-2012-1852 in Proceedings of the 53rd AIAA/ASME/ASCE/AHS/ASC Structures, Structural Dynamics and Materials Conference*, 2012.
- [30] A. NISSINEN, V. KOLEHMAINEN, AND J. P. KAIPIO, Reconstruction of domain boundary and conductivity in electrical impedance tomography using the approximation error approach, *Int. J. Uncert. Quant.*, 1(3):203–222, 2011.
- [31] A. PETRA, J. MARTIN, G. STADLER, AND O. GHATTAS, A computational framework for infinite-dimensional Bayesian inverse problems: Part II. Stochastic Newton MCMC with application to ice sheet flow inverse problems, *arXiv:1308.6221 e-prints*, 2013.
- [32] A. QUARTERONI, Numerical Models for Differential Problems, volume 8, Springer, MS&A Series, 2014.
- [33] A. QUARTERONI, G. ROZZA, AND A. MANZONI, Certified Reduced Basis Approximation for Parametrized Partial Differential Equations in Industrial Applications, *J. Math. Ind.*, 3(1), 2011.
- [34] O. RODERICK, M. ANITESCU, AND Y. PEET, Proper orthogonal decompositions in multifidelity uncertainty quantification of complex simulation models, *Int. J. Comput. Math.*, 91(4):748–769, 2014.
- [35] Y. SERINAGAOGLU, D. H. BROOKS, AND R. S. MACLEOD, Improved performance of Bayesian solutions for inverse electrocardiography using multiple information sources, *IEEE Trans. Biomed. Engng.*, 53(10):2024–2034, 2006.
- [36] A. M. STUART, Inverse problems: a Bayesian Perspective, *Acta Numer.*, 19(1):451–559, 2010.
- [37] A. TARANTOLA, Inverse Problem Theory and Methods for Model Parameter Estimation, *Society for Industrial and Applied Mathematics*, 2004.
- [38] D. XIU, AND J. S. HESTHAVEN, High-order collocation methods for differential equations with random inputs, *SIAM J. Sci. Comput.*, 27(3):1118–1139, 2005.

MOX Technical Reports, last issues

Dipartimento di Matematica “F. Brioschi”,
Politecnico di Milano, Via Bonardi 9 - 20133 Milano (Italy)

- 59/2014 MANZONI, A.; PAGANI, S.; LASSILA, T.
Accurate solution of Bayesian inverse uncertainty quantification problems using model and error reduction methods
- 58/2014 MENAFOGLIO, A.; SECCHI, P.; GUADAGNINI, A.
A Class-Kriging predictor for Functional Compositions with Application to Particle-Size Curves in Heterogeneous Aquifers
- 57/2014 GIVERSO, C.; VERANI, M.; CIARLETTA P.;
Branching instability in expanding bacterial colonies
- 56/2014 ANTONIETTI, P. F.; SARTI, M.; VERANI, M.; ZIKATANOV, L. T.
A uniform additive Schwarz preconditioner for the hp-version of Discontinuous Galerkin approximations of elliptic problems
- 55/2014 ANTONIETTI, P. F.; HOUSTON P.; SARTI, M.; VERANI, M.
Multigrid algorithms for hp-version Interior Penalty Discontinuous Galerkin methods on polygonal and polyhedral meshes
- 54/2014 FERRARIO, E.; PINI, A.
Uncertainties in renewable energy generation systems: functional data analysis, monte carlo simulation, and fuzzy interval analysis
- 53/2014 IEVA, F.; PAGANONI, A.M., PIETRABISSA, T.
Dynamic clustering of hazard functions: an application to disease progression in chronic heart failure
- 52/2014 DEDE , L.; QUARTERONI, A.; S. ZHU, S.
Isogeometric analysis and proper orthogonal decomposition for parabolic problems
- 51/2014 DASSI, F.; PEROTTO, S.; FORMAGGIA, L.
A priori anisotropic mesh adaptation on implicitly defined surfaces
- 50/2014 BARTEZZAGHI, A.; CREMONESI, M.; PAROLINI, N.; PEREGO, U.
An explicit dynamics GPU structural solver for thin shell finite elements